JBC RESEARCH ARTICLE

SPECC1L binds the myosin phosphatase complex MYPT1/PP1β and can regulate its distribution between microtubules and filamentous actin

Received for publication, September 23, 2022, and in revised form, December 19, 2022 Published, Papers in Press, January 10, 2023,
https://doi.org/10.1016/j.jbc.2023.102893

Virja Mehta[1,2], Nathalie Decan[1,2], Sarah Ooi[1,2], Antoine Gaudreau-Lapierre[1,2], John W. Copeland[1], and Laura Trinkle-Mulcahy[1,2,*]

From the [1]Department of Cellular and Molecular Medicine, Faculty of Medicine, University of Ottawa, Ottawa, Canada; [2]Ottawa Institute of Systems Biology, University of Ottawa, Ottawa, Canada

Edited by Enrique De La Cruz

The subcellular localization, activity , and substrate specificity of the serine/threonine protein phosphatase 1 catalytic subunit ($PP1_{cat}$) is mediated through its dynamic association with regulatory subunits in holoenzyme complexes. While some functional overlap is observed for the three human $PP1_{cat}$ isoforms, they also show distinct targeting based on relative preferences for specific regulatory subunits. A well-known example is the preferential association of MYPT1 with PP1β in the myosin phosphatase complex. In smooth muscle, MYPT1/PP1β counteracts the muscle contraction induced by phosphorylation of the light chains of myosin by the myosin light chain kinase. This phosphatase complex is also found in nonmuscle cells, where it is targeted to both myosin and nonmyosin substrates and contributes to regulation of the balance of cytoskeletal structure and motility during cell migration and division. Although it remains unclear how MYPT1/PP1β traffics between microtubule- and actin-associated substrates, our identification of the microtubule- and actin-binding protein SPECC1L in both the PP1β and MYPT1 interactomes suggests that it is the missing link. Our validation of their association using coimmunoprecipitation and proximity biotinylation assays, together with the strong overlap that we observed for the SPECC1L and MYPT1 interactomes, confirmed that they exist in a stable complex in the cell. We further showed that SPECC1L binds MYPT1 directly and that it can impact the balance of the distribution of the MYPT1/PP1β complex between the microtubule and filamentous actin networks.

Reversible protein phosphorylation is the most common posttranslational modification, acting as a molecular switch that can modulate protein conformation and/or protein–protein interactions. This in turn leads to alterations in enzymatic activity, subcellular localization, turnover of targets or signaling by other post-translational modifications (PTMs). Phosphoregulation plays a role in most cellular processes, including signaling, metabolism, migration, and cell cycle progression and is a key therapeutic target in diseases in which these processes are dysregulated. The predominant phosphorylated amino acid is serine (Ser), which accounts for >80% of phosphorylation events (1). Threonine (Thr) and tyrosine (Tyr) account for the bulk of the remaining phosphosites, with phosphorylation also demonstrated to a lesser extent on other amino acid residues (2). Protein phosphatase 1 (PP1) catalytic subunit ($PP1_{cat}$) is ubiquitously expressed in eukaryotic cells and estimated to account for up to 70% of Ser/Thr dephosphorylation events (3). Mammalian $PP1_{cat}$ is found primarily as three isoforms (α, β/δ, γ) that are encoded by three distinct genes (4). These isoforms are >89% identical in amino acid sequence, with minor variations primarily at their NH_2 and COOH termini (5). Loss of function and biochemical studies of individual PP1 isoforms in eukaryotic organisms suggest some level of compensation or overlapping function, while also highlighting distinct phenotypes associated with the disruption of a single gene (4).

In the cell, PP1 is regulated and achieves its substrate specificity through the association of the catalytic subunit with a range of regulatory or "targeting" subunits (6). This results in the combinatorial generation of a large and diverse group of dimeric PP1 holoenzyme complexes, each with its own subset of substrates and mechanism(s) of regulation. To date, >200 confirmed PP1-interacting proteins have been identified using a range of proteomic, bioinformatic, yeast two-hybrid, and biochemical approaches (7–13). The majority of known PP1 regulatory proteins contain an RVxF docking motif that mediates association with a hydrophobic pocket in $PP1_{cat}$ (14). Several contain additional PP1-binding sequences, such as SILK and MyPhoNE motifs, that enhance binding and contribute to isoform preference (see (6) for review). There is also a subset of inhibitory PP1 interactors that do not contain a typical RVxF docking motif (e.g., Inh2, SDS22) and can associate with PP1 bound to another regulatory subunit in trimeric complexes (6).

Our interactome screens comparing the three human PP1 phosphatase isoforms have identified and characterized numerous novel proteins not previously defined as phosphatase complex members (7, 9, 15). Of particular interest was the

* For correspondence: Laura Trinkle-Mulcahy, ltrinkle@uottawa.ca,

identification of the related Sperm antigen with calponin homology (CH) and coiled-coil domains 1 (SPECC1) and SPECC1L proteins, which were found to preferentially associate with PP1β yet possess no obvious PP1-binding motifs. This suggested that their interaction with PP1 is indirect, which was confirmed by their appearance in our MYPT1 interactome screens. MYPT1 is a regulatory subunit that binds preferentially to PP1β to generate the myosin phosphatase (MP) complex. Although most abundantly expressed in smooth muscle cells (15–17), it is found in many cell types, and targeted disruption of the Mypt1 gene in mice is embryonic lethal (18–20). In addition to its canonical role in regulating muscle contraction *via* dephosphorylation of myosin light chains, the MP complex plays a key role in the regulation of actomyosin in nonmuscle cells, affecting cell migration and adhesion (21). Several nonmyosin Mypt1/PP1β substrates have also been identified (for review see (22)). They include polo-like kinase 1 (PLK1), which MYPT1 associates with at centrosomes to contribute to mitotic regulation (23), and Histone Deacetylase 6 (HDAC6), which plays an important role in microtubule (MT) deacetylation (24).

Although not studied to the same extent, depletion of SPECC1L in cells led to defects in cytoskeletal organization, cell division, and migration (25, 26), and SPECC1L mutations have been linked to developmental facial morphogenesis disorders that result in congenital malformations (25, 27–30). The protein is found predominantly in the cytoplasm and has been shown to accumulate at both MT and filamentous actin structures throughout the cell cycle (25, 31). It is not yet clear how this distribution is regulated, as SPECC1L does not contain any obvious MT-binding domains. A single CH domain (32) at its C terminus may facilitate actin binding; however, 2 tandem CH domains are normally required to bind actin.

We confirmed that SPECC1L forms a stable complex with MYPT1 in nonmuscle cells, that the binding is direct, and that it is mediated by their respective C termini. Consistent with this, quantitative proteomic experiments demonstrated significant overlap of their interaction profiles, identifying proteins involved in the regulation of cell contractility, actin organization, MT stability, junction turnover, cytokinesis, adhesion, and migration. In addition to mapping the regions of SPECC1L that mediate association with MYPT1, MTs, and actin, we also demonstrated its ability to modulate the distribution of MYPT1/PP1β between these 2 cytoskeletal networks.

Results

SPECC1L/1 associate with the myosin phosphatase complex

As part of our ongoing analysis of PP1 holoenzyme complexes, we used our quantitative SILAC (stable isotope labeling by amino acids in culture) affinity purification/mass spectrometry (AP/MS) approach (33) to map the interactome of endogenous MYPT1 in U2OS cells (Fig. 1*A*) and compared the overlapping enriched proteins in 2 independent datasets (Fig. 1*B*; Supplemental Data File 1). As expected, we saw strong enrichment of both PP1β and the myosin regulatory light chain, along with numerous proteins related to motility and cytoskeletal organization. We also observed strong enrichment of SPECC1L and further confirmed their association by demonstrating coprecipitation of endogenous MYPT1 with GFP-tagged SPECC1L (Fig. 1*C*). An interesting observation was that not only did endogenous SPECC1L coprecipitate with transiently overexpressed GFP-tagged MYPT1 in the reciprocal experiment (Fig. S1*A*) but also it was the only protein besides PP1β that was significantly enriched (Fig. S1*B*). We had previously observed that transient overexpression of bait proteins at high levels for AP/MS-based interactome mapping can hamper incorporation into endogenous signaling complexes as binding sites saturate, although high-affinity binary interactors are usually detected (34). While we were carrying out these experiments, a SPECC1L-MYPT1 association was also annotated in a large-scale screen for phosphatase interactors (13), although it was not further explored in that study.

Enrichment of the related family member SPECC1 was also detected in one of the endogenous MYPT1 datasets (Supplemental Data File 1), and their association was validated by coimmunoprecipitation of MYPT1 with GFP-tagged SPECC1 (Fig. 1*C*). In a complementary BioID approach (35), we demonstrated biotin-based proximity labeling of MYPT1 in cells expressing either SPECC1L (Fig. 1*D*) or SPECC1 (Fig. 1*E*) fused to the biotin ligase BirA*.

We next mapped the interactome of SPECC1L in U2OS cells, to compare its overlap with that of MYPT1. As none of the available commercial antibodies were suitable for immunoprecipitation, we established a U2OS cell line stably overexpressing GFP-tagged SPECC1L at endogenous levels (Fig. 1*G*) and confirmed that its subcellular localization matched that of the endogenous protein (Fig. 1*F*, Fig. 4, *A* and *B*). Fig. 1*H* shows a comparison of the SPECC1L-GFP and MYPT1 interactomes. As highlighted in the Venn diagram, the high-confidence hits (top right quadrant in the graph) show strong overlap, with 76% of the SPECC1L interactors identified in the MYPT1 dataset and 43% of the MYPT1 interactors identified in the SPECC1L dataset. These overlapping factors, listed in the color-coded table (Fig. 1*I*), are involved in the regulation of cell contractility, actin organization, MT stability, junction turnover, cytokinesis, adhesion, and migration. A Gene Ontology Enrichment Analysis (36) is included in Supplemental Data File 1. Although PP1β was just below our stringent >2-fold enrichment threshold in the SPECC1L dataset, we confirmed their association by IP/WB analysis (Fig. S1*C*).

MYPT1 directly interacts with SPECC1L via *their respective C termini*

Using GlobPlot2.3 (http://globplot.embl.de/) (37) to predict regions of disorder and globularity, we designed a truncation mutant strategy to probe for the association of specific regions

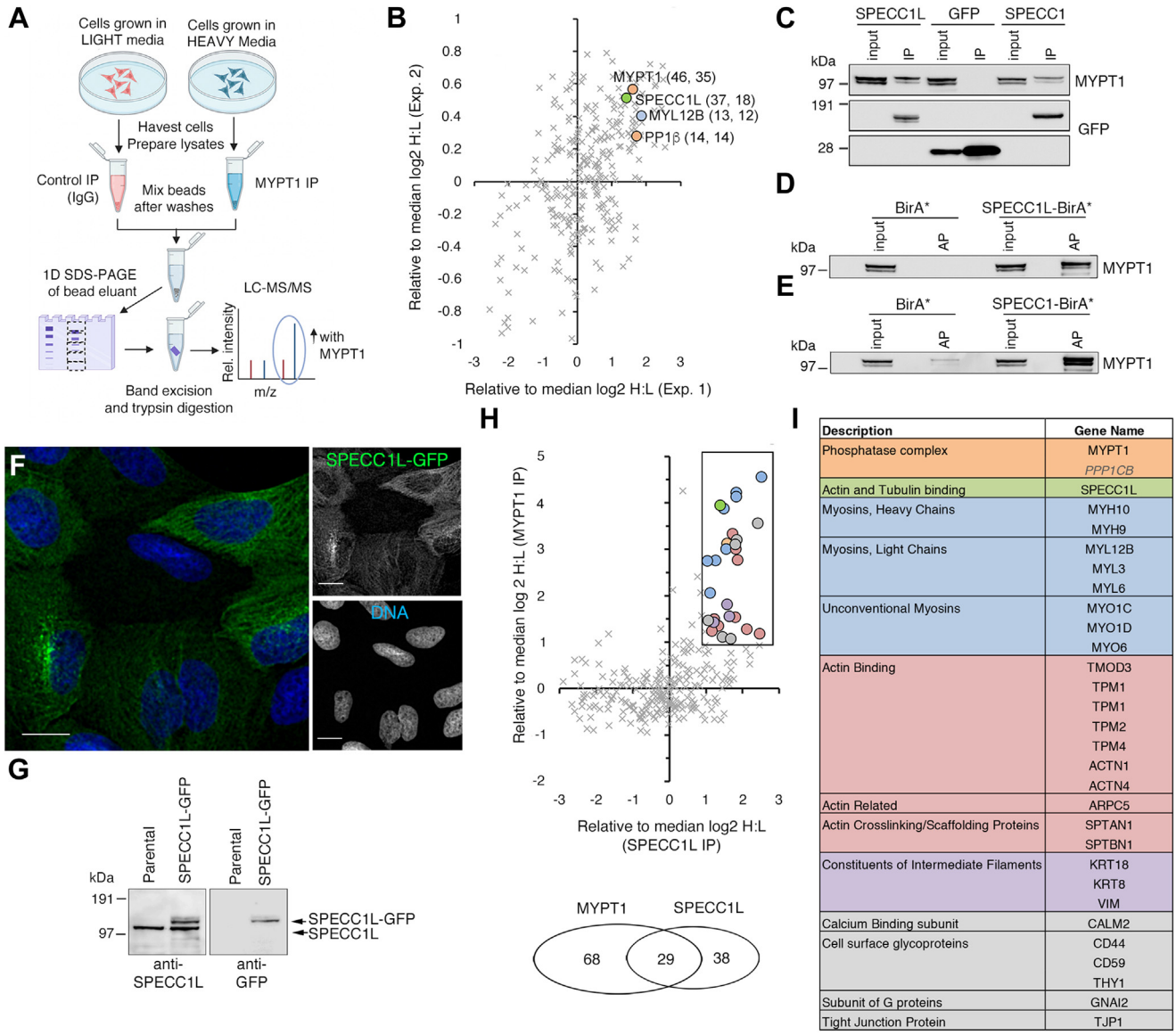

Description	Gene Name
Phosphatase complex	MYPT1
	PPP1CB
Actin and Tubulin binding	SPECC1L
Myosins, Heavy Chains	MYH10
	MYH9
Myosins, Light Chains	MYL12B
	MYL3
	MYL6
Unconventional Myosins	MYO1C
	MYO1D
	MYO6
Actin Binding	TMOD3
	TPM1
	TPM1
	TPM2
	TPM4
	ACTN1
	ACTN4
Actin Related	ARPC5
Actin Crosslinking/Scaffolding Proteins	SPTAN1
	SPTBN1
Constituents of Intermediate Filaments	KRT18
	KRT8
	VIM
Calcium Binding subunit	CALM2
Cell surface glycoproteins	CD44
	CD59
	THY1
Subunit of G proteins	GNAI2
Tight Junction Protein	TJP1

Figure 1. SPECC1L associates with the myosin phosphatase complex and shows an overlapping interactome enriched in cytoskeletal factors. *A.* design of the SILAC AP/MS experiment used to map the interactome of endogenous MYPT1. *B.* graph showing factors enriched in two replicates of the AP/MS experiment (upper right quadrant), plotted as the displacement from the median log2 H:L ratio in both. For the highlighted proteins, the number of peptides detected in each experiment is noted in parentheses. *C.* GFP-tagged SPECC1L and SPECC1 immunoprecipitated from U2OS cells copurify endogenous MYPT1. Proximity biotin labeling of endogenous MYPT1 by Myc-BirA*-SPECC1L and Myc-BirA*-SPECC1 expressed in U2OS cells allows it to be captured on Streptavidin-agarose beads and visualized by Western blot analysis with anti-MYPT1 (*D–E*). *F.* field of view of U2OS cells stably overexpressing SPECC1L-GFP (green). Hoechst 33342-stained DNA is shown in blue. The scale bar represents 10 μm. *G.* Western blot analysis with anti-SPECC1L (left panel) and anti-GFP (right panel) antibodies shows that the U2OS$^{SPECC1L\text{-}GFP}$ stable line expresses the fusion protein at a similar level to the endogenous protein. *H.* factors enriched >2-fold in both MYPT1 and SPECC1L SILAC AP/MS experiments are highlighted on the graph (upper right quadrant) and color-coded table (*I*). PP1β (in italics) was just below the 2-fold enrichment threshold in the SPECC1L experiment. The Venn diagram shows the number of factors that overlap. The full datasets are provided in Supplemental Data File 1. AP/MS, affinity purification/mass spectrometry; SILAC, stable isotope labeling by amino acids in culture.

of both proteins and determine whether or not their interaction is direct. We first assessed coprecipitation of endogenous MYPT1 from cell lysates with GFP-tagged SPECC1L truncation mutants (Fig. 2*A*). Our results indicated that the C-terminal half of SPECC1L (SPECC1L-CT; aa 462–1117) mediates its association with MYPT1, as confirmed both by IP/WB (Fig. 2*B*) and BioID (Fig. 2*C*). Similarly, the C-terminal half (aa 462–1068) of the related family member SPECC1 governs its association with MYPT1 (Fig. 2*G*). Further truncation of the C terminus of SPECC1L (ΔNTΔCHD) revealed that the C-terminal actin-binding CH domain is not required for MYPT1 association (Fig. 2*B*).

To determine which region(s) of MYPT1 mediate its association with SPECC1L, we divided the protein into three fragments: an N-terminal region containing the PP1-binding RVxF motif followed by a series of ankyrin repeats (ANK; aa 1–344), a middle region (MID; aa 345–653), and a C-terminal region that contains a coiled-coil domain (CCD) and leucine zipper (LZ) domain (CD; aa 654–1030) (Fig. 2*D*). The localization of the fragments is consistent with previous reports that

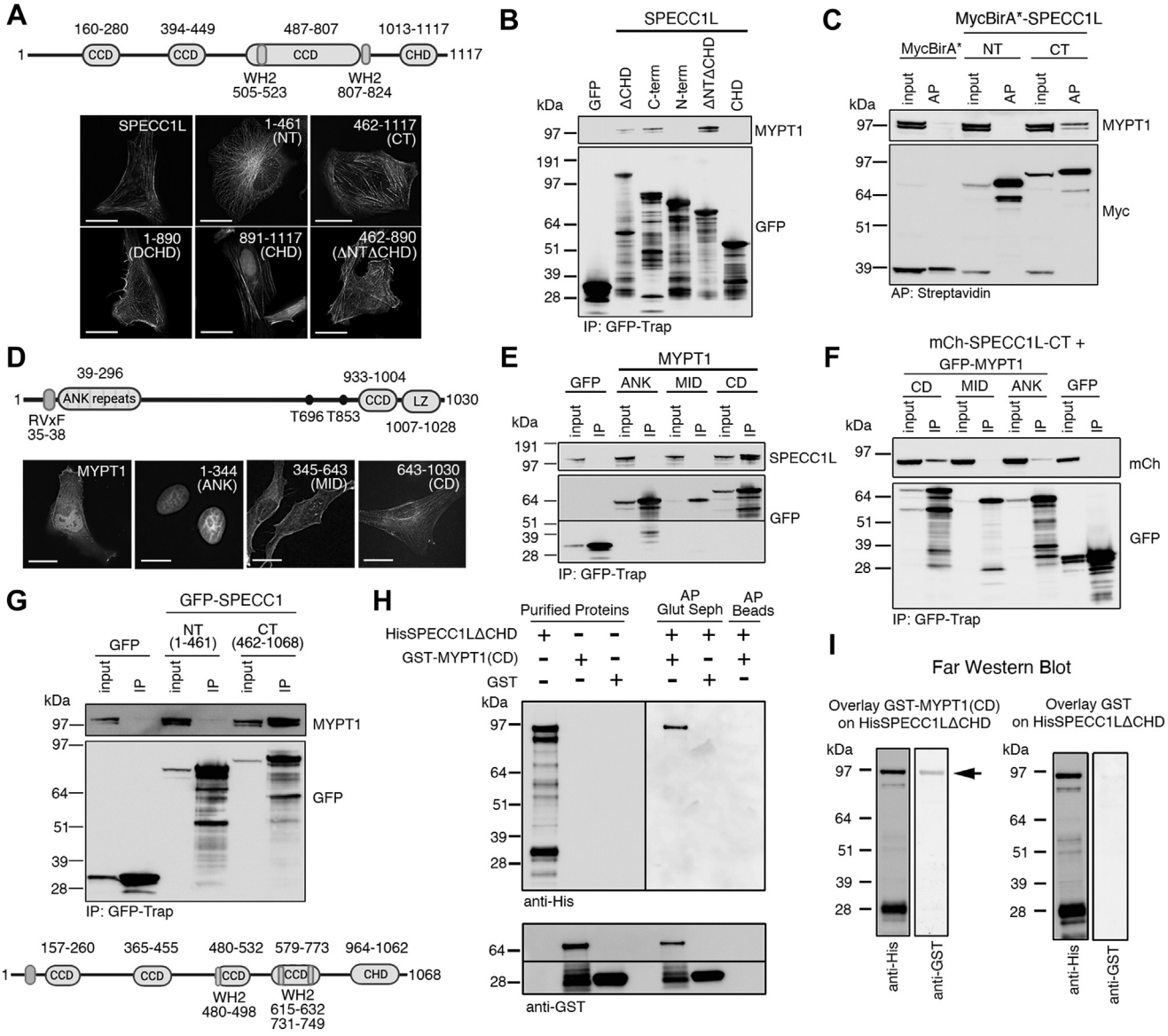

Figure 2. SPECC1L binds MYPT1 directly. *A*. SPECC1L contains three coiled-coil domains (CCD), A C-terminal calponin homology domain (CHD), and two putative WASP homology domain-2 (WH2) actin-binding domains. Various truncation mutants exhibit distinct subcellular localizations. The scale bars represent 10 μm. The minimal region of SPECC1L required for association with MYPT1 is ΔNTΔCHD (aa 462–890), which contains the third CCD. This was demonstrated both by coimmunoprecipitation of endogenous MYPT1 with GFP-tagged SPECC1L fragments (*B*) and by BioID using BirA*-tagged N- and C-terminal fragments (*C*). *D*. MYPT1 consists of a series of N-terminal ankyrin repeats adjacent to an RVxF PP1-binding motif and C-terminal coiled-coil and leucine zipper (LZ) domains. Three truncation mutants (ANK, aa 1–344; MID, aa 345–643; CD, aa 643–1030) based on the literature demonstrate the expected subcellular localization patterns. The scale bars represent 10 μm. The minimal region of MYPT1 required for association with SPECC1L is the CD region, which includes the CCD and LZ domain. This was shown both by coimmunoprecipitation of endogenous SPECC1L with GFP-tagged MYPT1 fragments (*E*) and by coimmunoprecipitation of mCh-tagged SPECC1L-CT with GFP-tagged MYPT1 fragments (*F*). The C-terminal half of SPECC1 also governs its association with MYPT1, as shown by copurification of endogenous MYPT1 with GFP-SPECC1-CT (*G*). Recombinant His-SPECC1LΔNTΔCHD binds recombinant GST-MYPT1(CD) directly in both *in vitro* coprecipitation (*H*) and far Western blot (*I*) assays. GST alone is used as a negative control for both.

show GFP-MYPT(ANK) to be nuclear, (MID)Mypt1-GFP to be both nuclear and cytoplasmic, and GFP-Mypt1(CD) to be predominantly cytoplasmic in association with the cytoskeleton (38). When affinity purified from cell lysates, only MYPT1(CD) copurified with endogenous SPECC1L (Fig. 2*E*). This region also mediates association with known interactors that include myosin, the active form of RhoA, the M20 MP subunit, and the inhibitory CPI-17 protein (see (22) for review). Finally, we confirmed that, when coexpressed in cells, GFP-MYPT1(CD) copurifies with mCherry-tagged SPECC1L-CT (Fig. 2*F*).

We next set out to determine if SPECC1L directly binds MYPT1. To do this, we first expressed and purified recombinant GST-MYPT1(CD). Recombinant SPECC1L-CT was more susceptible to degradation, so we tested all of the fragments and chose to work with SPECC1LΔCHD (1–890), which is a close representation of the full-length protein that retains MYPT1 association (Fig. 2*B*). Recombinant His-SPECC1LΔCHD was mixed with recombinant GST-MYPT1(CD) or GST alone, which were then captured on Glutathione Agarose beads for detection of copurified HisSpecc1LΔCHD by WB analysis using anti-His antibodies (Fig. 2*H*). This *in vitro* coprecipitation assay

confirmed direct and specific interaction of His-SPECC1LLΔCHD with GST-MYPT1(CD). In a complementary far WB approach, purified His-SPECC1LΔCHD was resolved on a 1D SDS-PAGE gel, transferred to a nitrocellulose membrane, and overlaid with either purified GST-MYPT1(CD) or GST alone. Fig. 2*I* shows the specific and direct binding of GST-MYPT1(CD) to His-SPECC1LΔCHD.

Distinct regions of SPECC1L mediate its association with microtubules and actin filaments

The distinct subcellular localizations observed for the various SPECC1L truncation mutants (Fig. 2*A*) were consistent with previous results suggesting that SPECC1L associates with both the MT network and the actin cytoskeleton (25, 26, 31). We first confirmed that the network at which the N-terminal half (SPECC1L-NT; aa 1–461) accumulates counterstained with anti-α-tubulin (Fig. 3*A*). This localization pattern was lost when cells were treated with the polymerization inhibitor nocodazole (NOC) to disrupt the MT network (Fig. 3*A*, bottom panels). We therefore concluded that this region of SPECC1L mediates MT association.

In order to test whether this association is direct or indirect, we performed a MT-binding protein spin-down assay. Purified recombinant His-tagged SPECC1L-NT was mixed with freshly prepared MTs and the reaction mix centrifuged at 100,000*g*. At this speed, the MTs pellet along with any protein that directly associates with them. SPECC1L-NT was observed to specifically pellet in the presence of MTs and remained in the supernatant in their absence (Fig. 3*C*; Fig. S1*D*). Bovine serum albumin (BSA) was included as a negative control, as it does not bind MTs and thus remains in the soluble fraction, while the known MT-binding protein MAP4 was included as a positive control. This assay confirms, for the first time, that SPECC1L is a *bona fide* MT-binding protein.

The presence of a CH domain (32) at the C terminus of SPECC1L (Fig. 2*A*) has been suggested to facilitate actin binding. Our analysis using the ELM (eukaryotic linear motif) online resource (39) also identified 2 putative WH2 actin-binding domains in the C-terminal half of SPECC1L, upstream of the CH domain (Fig. 2*A*). We first confirmed that the structures at which SPECC1L-CT accumulates counterstain with fluorophore-tagged phalloidin, a high-affinity probe for filamentous (F)-actin (Fig. 3*B*). This localization pattern was lost when cells were treated with Latrunculin B (LAT), which sequesters monomeric G-actin and induces disassembly of actin filaments (Fig. 3*B*, bottom panels). Using a standard actin fractionation approach (40), we further demonstrated that GFP-tagged SPECC1L-CT expressed in U2OS cells is resistant to Triton X-100 extraction, remaining in the insoluble cytoskeletal fraction with F-actin (Fig. 3*D*). The nonpolymerizable actin R62D mutant (41) was included to demonstrate its shift to soluble (G-actin) pools.

To test the contributions of the predicted actin-binding regions to this localization, we removed either the CH domain (ΔNTΔCHD; aa 461–890) or the WH2 domains (CHD; aa 890–1117) from the C-terminal half of SPECC1L. Removal of the CH domain did not obviate actin association (Fig. 3*E*), although the pattern differs from that observed for the CH domain–containing fragment (Fig. 3*F*). While the CHD derivative distributes along straight stretches of a filamentous network, the ΔNTΔCHD mutant associates with both cortical filaments and in shorter structures in the cytoplasm. Both localization patterns are disrupted with LAT but not NOC treatment (Fig. 3, *E* and *F*, bottom panels), confirming that they represent accumulations at actin structures. This suggests that both regions play roles in the targeting of SPECC1L to the actin network, possibly by mediating association with specific actin structures.

Overexpression of SPECC1L induces stabilized and acetylated microtubule bundles

Consistent with previous reports in the literature (25, 42), immunofluorescence analysis of endogenous SPECC1L shows overlap with the MT and F-actin networks during interphase, although the latter predominates (Fig. 4*A*). This was also observed for SPECC1L-GFP stably overexpressed at endogenous levels in U2OS cells (Fig. 4*B*). Interestingly, removing the CH domain shifts this pattern, with the SPECC1L-ΔCHD truncation mutant demonstrating both filamentous-actin and MT pools (Fig. 3*G*). This suggests a dynamic balance of distribution between these 2 networks that is regulated, at least in part, by competition between MT-binding and actin association domains.

Expression of increasingly higher levels of full-length SPECC1L resulted in aberrant accumulation in thick, thread-like structures (Fig. 4*C*). These structures counterstain with antibodies that detect both alpha-tubulin or its acetylated (on K40) form, the latter of which is a marker for stabilized MTs (Fig. 4*D*; (43)). They are also sites of accumulation of the Tau family Microtubule Associated Protein 4 (MAP4; Fig. 4*E*), which has been shown to promote MT stabilization and regulate MT-based motility (44).

The thickness of the structures suggested bundling of multiple MTs, which we assessed by super-resolution imaging. First, we used an X10 Expansion Microscopy approach (45, 46) to isotropically expand U2OS cells transiently overexpressing SPECC1L-GFP that had been fixed and stained with anti-GFP (to boost the SPECC1L signal) and anti-acetylated-alpha-tubulin antibodies. Airyscan-based imaging of gel segments using a Zeiss LSM880 confocal laser scanning microscope confirmed that the thick structures represent multiple closely associated MT strands lying in parallel (Fig. 4*F*). This was also observed when we used a complementary direct stochastic optical reconstruction microscopy super-resolution imaging approach (47) to visualize the acetylated tubulin signal in regions of SPECC1L-GFP accumulation (Fig. 4*G*). Interestingly, we did occasionally observe transient accumulation of SPECC1L-GFP at MT bundles in our stable cell line, with live imaging showing that it could reverse over time (Fig. S1*E*). This is consistent with the idea that a localized elevated level of SPECC1L, which can associate with both the actin cytoskeleton and the MT network, has the potential to impact the homeostatic balance of cytoskeletal organization in cells.

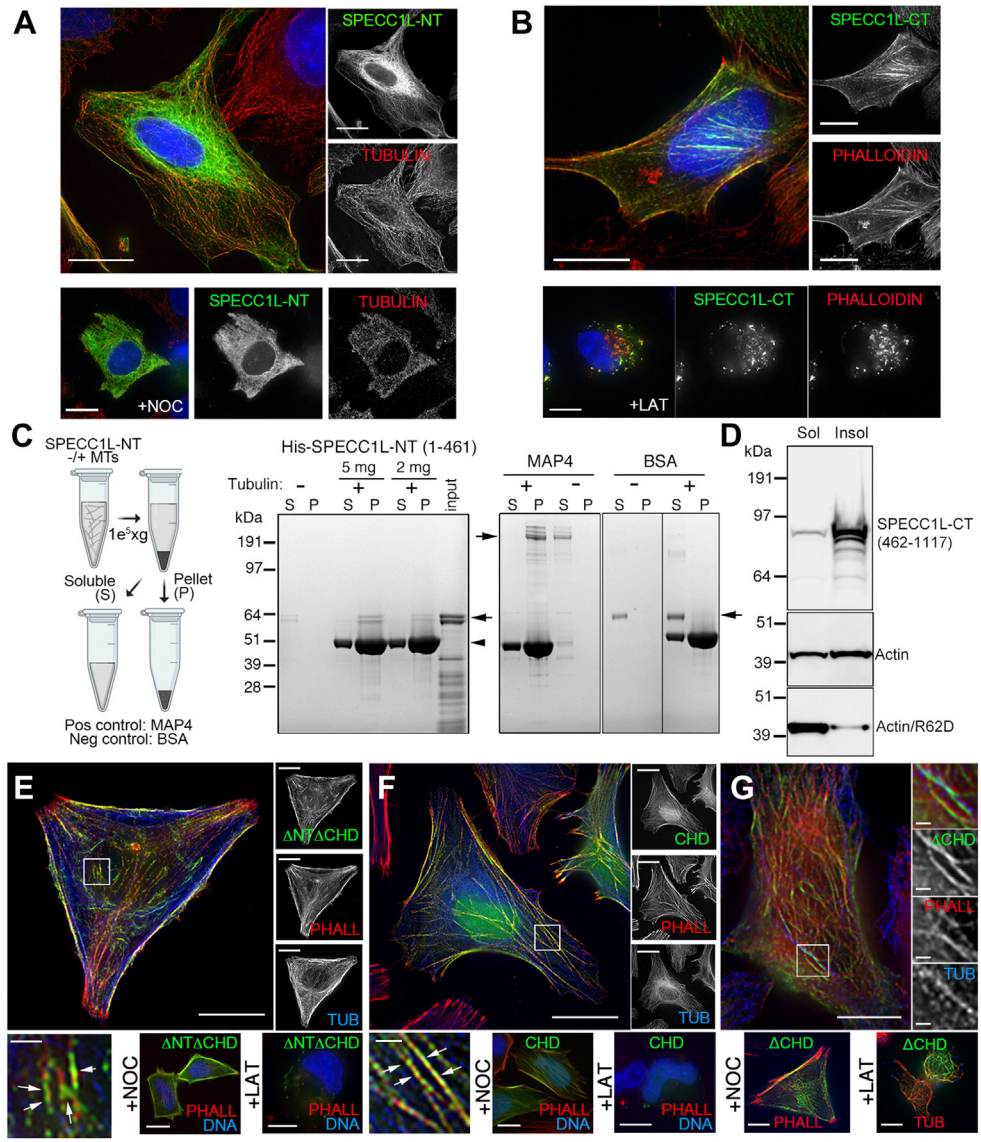

Figure 3. Distinct regions of SPECC1L mediate its association with microtubules and actin filaments. *A*. the N-terminal half (NT; aa 1–461; green) of SPECC1L associates with microtubules that counterstain with anti-alpha-tubulin-Alexa Fluor 568 (red) in U2OS cells, and this localization is disrupted with nocodazole (NOC) treatment (8.3 μM for 2 h). Hoechst 33342-stained DNA is shown in blue. *B*. the C-terminal half (CT; aa 461–1117; *green*) of SPECC1L associates with actin filaments that counterstain with Alexa Fluor 568–Phalloidin (*red*), and this localization is disrupted with latrunculin B (LAT) treatment (2 μM for 2 h). Hoechst 33342-stained DNA is shown in blue. *C*. purified SPECC1L-NT binds microtubules directly in a microtubule binding assay, showing an enrichment (*arrow*) in the pellet (P) *versus* the supernatant (S) fraction when tubulin (*arrowhead*) is included in the assay. Coomassie-stained gels are shown here, while Western blot detection of His-SPECC1L and Tubulin in the same assay is shown in Fig. S2. The microtubule-binding protein MAP4 was included as a positive control and bovine serum albumin (BSA) as a negative control. *D*. in an actin fractionation assay, the majority of SPECC1L-CT remains in the insoluble fraction with filamentous actin when U2OS cells are extracted with Triton X-100. The nonpolymerizable Actin R62D mutant, which remains soluble, is included as a negative control. SPECC1L was detected using anti-GFP antibodies and Flag-Actin (WT and R62D) was detected using anti-Flag antibodies. SPECC1L ΔNTΔCHD (*E*) and SPECC1L-CHD (*F*) both colocalize with phalloidin-stained F-actin structures (red; see arrows in enlarged insets) in U2OS cells, albeit with different localization patterns. Tubulin staining is shown in *blue*. These structures are disrupted with LAT but not NOC treatment. *G*. SPECC1L lacking the CHD (*green*) shows overlap with both stained microtubules (anti-tubulin; *blue*) and actin filaments (phalloidin; *red*) and demonstrates both a LAT-resistant MT pool and an NOC-resistant actin filament pool. All scale bars represent 10 μm.

It is important to note that MT bundling is only observed with overexpression of full-length SPECC1L. Even at very high levels of overexpression, the MT-binding region alone (SPECC1L-NT) only accumulates at MTs and does not induce bundling, suggesting contributions from the actin and/or MYPT1 association domains to this phenotype. Similarly, removal of the C-terminal actin-binding CH domain (SPECC1L-ΔCHD) promotes increased association with MTs (Fig. 3*G*) but does not promote the thick, bundled MT phenotype (25).

Sequence alignment of the N-terminal regions (aa 1–461) in SPECC1L and SPECC1 identified a stretch within their respective second coiled-coil domains that shows a high degree of similarity between the 2 proteins (Fig. 7*C*). Mutations in this region in SPECC1L have been identified in patients with the congenital developmental disorders Opitz G/BBB and Teebi hypertelorism (27–30) (Fig. 7*B*), and previous studies suggested that disrupted MT association may contribute to the observed phenotypes. Although we did not detect changes in MT association or the stabilization/

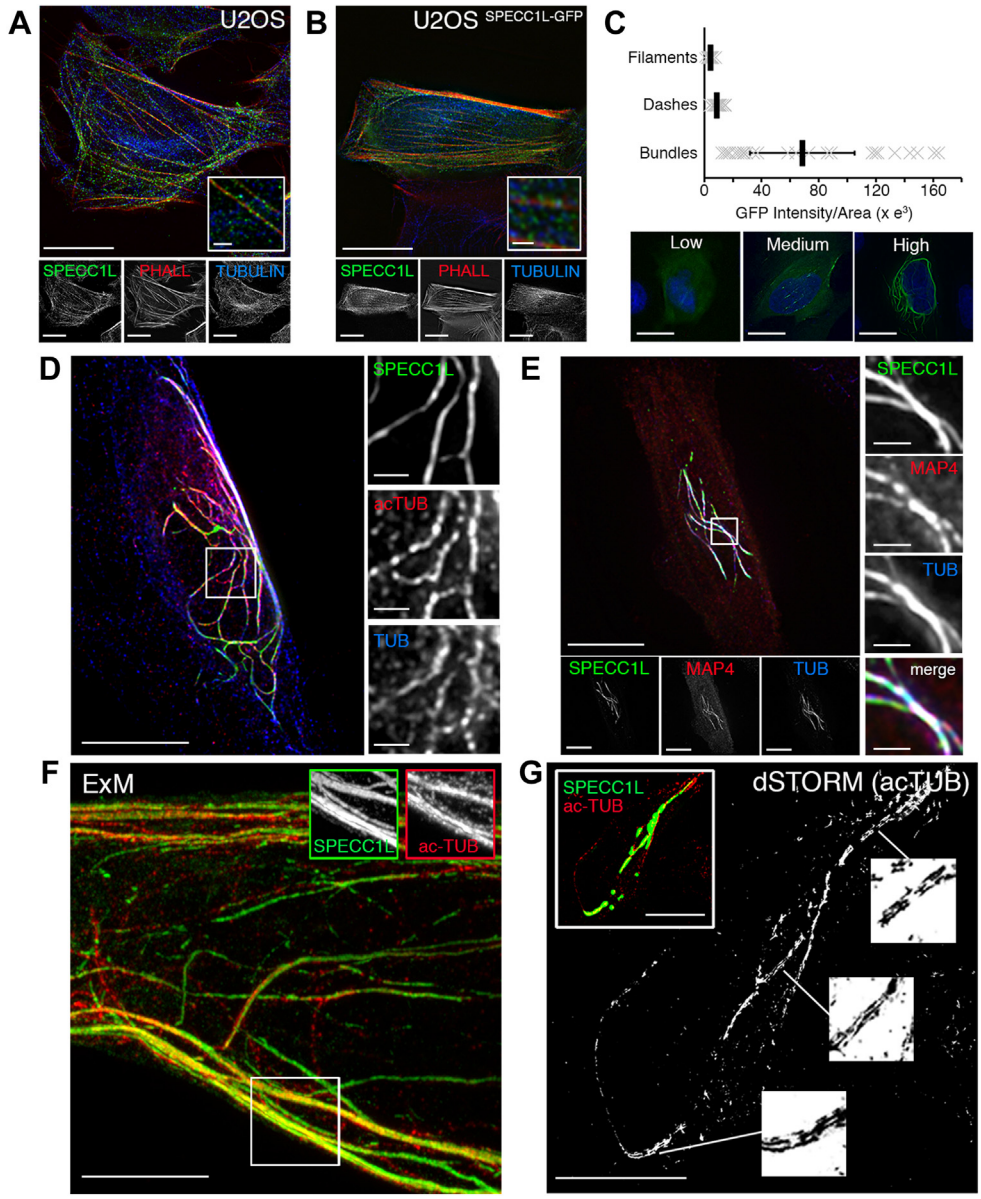

Figure 4. Overexpression of SPECC1L induces stabilized and acetylated microtubule (MT) bundles. *A.* in untreated interphase U2OS cells, the localization of endogenous SPECC1L detected by immunostaining (*green*) is predominantly cytoplasmic and overlaps the phalloidin-stained F-actin pattern (*red*) more closely than the MT pattern detected by anti-alpha-tubulin staining (*blue*). *B.* a similar pattern is observed for SPECC1L-GFP stably expressed at endogenous levels in the U2OS$^{SPECC1L\text{-}GFP}$ cell line. *C.* overexpression of SPECC1L at increasingly higher levels shifts localization from predominantly filamentous to accumulation in cytoplasmic "dashes" (at medium intensities) and "bundles" (at high intensities). GFP intensities and localization were annotated for >60 cells in three independent experiments (bar = mean ± SE). *D.* cytoplasmic SPECC1L bundles (*green*) counterstain with antibodies against both alpha-tubulin (*blue*) and alpha-tubulin acetylated on Lys40 (acTUB; *red*). *E.* mCh-MAP4 (*red*) accumulates at SPECC1L-GFP (*green*) MT bundles counterstained with anti-alpha-tubulin (*blue*). Analysis of these SPECC1L/acetylated MT bundles at nanoscale resolution by expansion microscopy (ExM; *F*) and direct stochastic optical reconstruction microscopy single molecule localization microscopy (*G*) confirmed that the thick structures consist of multiple MTs aligned in parallel and in close association. All scale bars represent 10 μm.

bundling phenotype for 2 of these mutations (T397P and Q415P) when introduced into SPECC1L or SPECC1L-NT, it may be that the impact is subtle and effects accumulate over time. A more recent study reported diminished overlap with MTs when the entire CCD2 was removed (42). Functional MT binding may also require additional regions in the N-terminal half of the protein. SPECC1 is expressed as multiple splice variants, and we have compared SPECC1 isoform 1 (NSP5b3b) with SPECC1L as they are the most similar in size and structure. There is, however, a splice variant (isoform 4; NSP5a3b) in which the N-terminal residues 1 to 94 are replaced by a unique stretch of 13 aa (Fig. 7*C*). Interestingly, although SPECC1/iso1 shows the same MT bundling phenotype as SPECC1L (Fig. S3*D*), SPECC1/iso4 remains predominantly associated with actin filaments, even at high levels of overexpression (Fig. S3*E*). Although SPECC1/iso1 contains a potential KxGS MT-binding domain within its unique N terminus that is similar to those found in the MT-binding domains of Tau, MAP2C, and MAP4 (Fig. 7*C*) and conserved in SPECC1L as KxGT (Fig. 7*B*), this 94-aa region of SPECC1 was not sufficient to promote MT association on its own when fused to GFP.

SPECC1L modulates the subcellular distribution and turnover dynamics of the myosin phosphatase complex

To determine whether overexpression of full-length SPECC1L can also shift the balance of MYPT1 localization, we stained cells transiently overexpressing SPECC1L-GFP with anti-MYPT1 antibodies and confirmed that a pool of endogenous MYPT1 is recruited to the SPECC1L-containing MT bundles (Fig. 5*A*). We next assessed effects on the localization and turnover dynamics of MYPT1 in a HeLa bacterial artificial chromosome cell line that drives expression of GFP-tagged mouse Mypt1 (91.7% identical to the human protein) under the control of its endogenous promoter (48). For these experiments, we expressed BirA*-tagged SPECC1L, which allowed us to compare the localization of Mypt1-GFP to the proximity labeling profile of SPECC1L detected with fluorophore-tagged streptavidin. This confirmed that all cells that showed a bundled MT phenotype with Mypt-GFP were also expressing the SPECC1L fusion protein (Fig. 5*B*). Similarly, coexpression of BirA*-tagged SPECC1L-CT induced a visible increase in accumulation of Mypt1-GFP on F-actin (Fig. 5*C*).

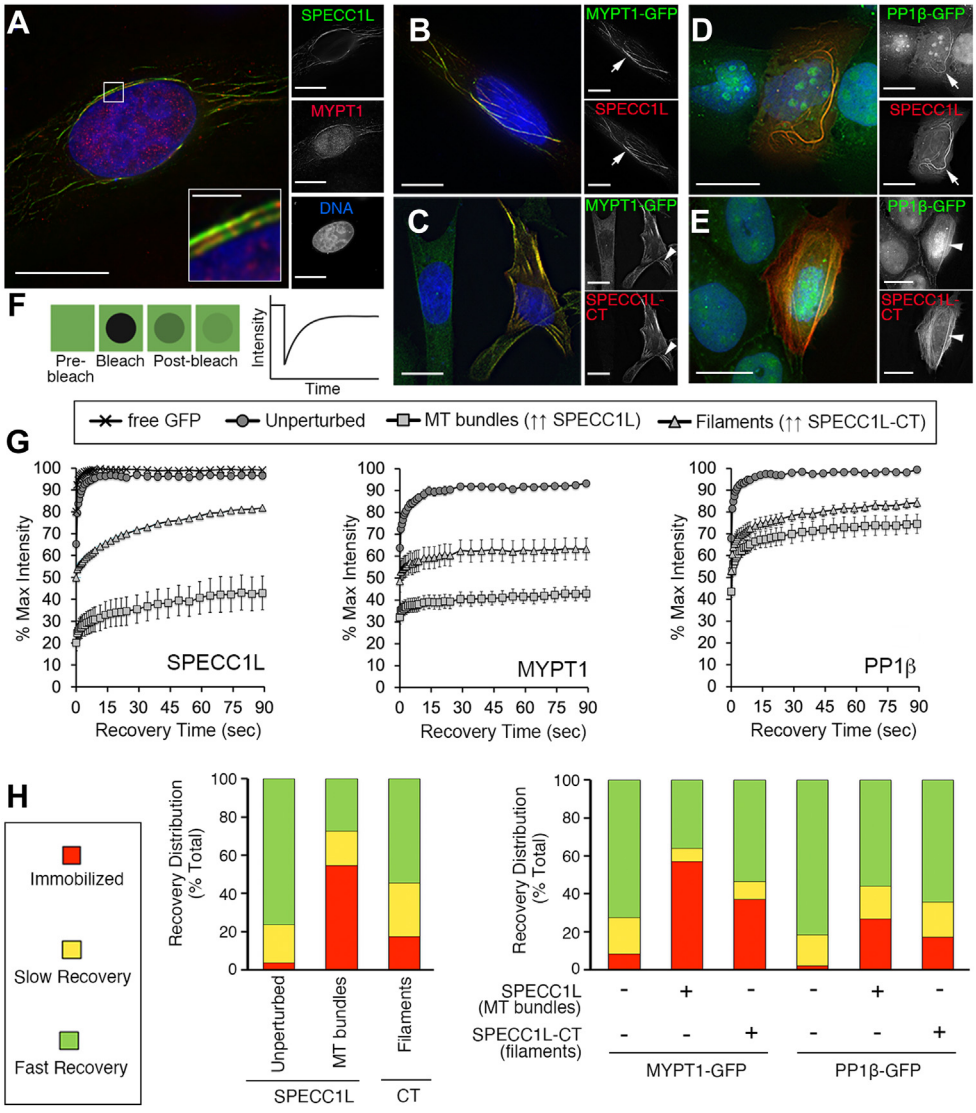

Figure 5. SPECC1L modulates the subcellular distribution and turnover dynamics of the myosin phosphatase complex. *A*. endogenous MYPT1 (*red*) accumulates at the bundled/stabilized microtubules (MTs) induced by transient overexpression of SPECC1L-GFP (*green*). The scale bar represents 10 μm (for enlarged inset the scale bar represents 1 μm). Mypt1-GFP (*green*) in the bacterial artificial chromosome HeLa line is recruited to MT bundles induced by transient overexpression of SPECC1L-BirA* (*B*, *arrows*), and to actin filaments at which transiently overexpressed SPECC1L-CT accumulates (*C*, *arrowheads*). Biotinylation patterns were detected using Alexa Fluor 647–tagged Streptavidin (*red*). Hoechst 33342-stained DNA is shown in blue. The scale bars represent 10 μm. PP1β-GFP (*green*) in the U2OS$^{PP1β-GFP}$ stable line is recruited to MT bundles induced by transient overexpression of SPECC1L (*D*, *arrows*) and to actin stress fibers at which transiently overexpressed SPECC1L-CT accumulates (*E*, *arrowheads*). Biotinylation patterns were detected using Alexa Fluor 647–tagged Streptavidin (red). Hoechst 33342-stained DNA is shown in *blue*. The scale bars represent 10 μm. *F*. cartoon diagram summarizing the design of the fluorescence recovery after photobleaching (FRAP) experiments. Following a prebleach image, the GFP in a region of interest is photobleached at 100% laser power and recovery of signal in the region of interest monitored over time (90 s post bleach). *G*. FRAP curves for GFP-tagged SPECC1L- and SPECC1L-CT (unperturbed represents SPECC1L-GFP in the U2OS $^{SPECC1L-GFP}$ stable line) and for Mypt1-GFP and PP1β-GFP either unperturbed or at the structures to which they are recruited by overexpressed SPECC1L or SPECC1L-CT (as shown in *A*–*B*). *H*. tables summarizing the FRAP results, based on mobile fractions and recovery times calculated using GraphPad Prism (Table S1). In all cases, the recovery curves for the mobile fraction were best fit by a double exponential line, indicating 2 pools with different recovery times (slow and fast). Representative FRAP experiments are shown in Fig. S2.

Given that SPECC1L copurifies MYPT1/PP1β as a complex (Fig. S1*C*; Supplemental Data File 1), we reasoned that SPECC1L-induced relocalization of Mypt1 would be accompanied by a concomitant change in the localization of PP1β. For these experiments we utilized a U2OS cell line that stably expresses a low level of GFP-tagged PP1β. We demonstrated that overexpression of full-length SPECC1L recruits a pool of PP1β-GFP to bundled MTs (Fig. 5*D*), while overexpression of the C-terminal half recruits excess PP1β-GFP to actin filaments (Fig. 5*E*).

Having confirmed that relocalization of both GFP-tagged Mypt1 and PP1β is sufficiently pronounced to allow us to unambiguously identify non-fluorophore-tagged SPECC1L and SPECC1L-CT-expressing cells based on their altered subcellular localization patterns, we set out to assess their turnover dynamics by fluorescence recovery after photobleaching (FRAP) analysis in live cells. In these experiments, the pool of GFP in a region of interest (ROI) in the cell is irreversibly photobleached using a high-powered 488-nm laser, and the return of a GFP signal to this ROI (which represents exchange with pools of GFP outside the ROI) is monitored over time (Fig. 5*F*). Recovery profiles that are slower and less complete than that observed for free GFP over the same time scale suggest association with underlying subcellular structures/complexes.

Analysis of cytoplasmic SPECC1L-GFP in the stable cell line revealed that the fusion protein is relatively dynamic, albeit with slower turnover dynamics compared with GFP alone (Fig. 5*G*, left graph, circles *versus* crosses). Overexpressed SPECC1L-GFP that accumulated at bundled MTs has a significantly reduced mobile fraction with a slower recovery rate (Fig. 5*G*, left graph, squares), suggesting near immobilization at these structures. As previously noted, the N-terminal half of SPECC1L, when overexpressed as a GFP fusion in cells, accumulates on the MT network (Fig. 3*A*) but does not induce bundling/stabilization. Assessment of its turnover dynamics by FRAP revealed full recovery within 90 s post bleach, albeit at a slower recovery rate than free GFP (∼1 s *versus* <0.001 s), suggesting a normal on/off association with MTs. This again suggests that the bundling/stabilization phenotype requires a specific region within the C-terminal half of the protein.

Mypt1-GFP also showed a reduced mobile fraction and slower turnover rate compared with free GFP, confirming the presence of underlying binding events (Fig. 5*G*, middle graph, circles). Overexpression of full-length SPECC1L induced accumulation of a pool of Mypt1-GFP at bundled MTs and a dramatic reduction in its turnover dynamics at these structures (Fig. 5*G*, middle graph, squares), similar to the near immobilization observed for SPECC1L-GFP. PP1β-GFP also showed slower turnover dynamics than free GFP (Fig. 5*G*, right graph, circles), and its mobility changed significantly when it was recruited to MT bundles by overexpressed full-length SPECC1L (Fig. 5*G*, right graph, squares). Representative FRAP experiments for SPECC1L-GFP, Mypt1-GFP, and PP1β-GFP at MT bundles are shown in Fig. S2*A*.

FRAP analysis of the C-terminal SPECC1L fragment, which accumulates at actin filaments (Fig. 3), also showed a significantly reduced mobile fraction and slower turnover rate (Fig. 5*G*, left graph, triangles). Consistent with this observation, reduced mobile fractions and slower turnover rates were observed for the pools of excess Mypt1-GFP (Fig. 5*G*, middle graph, triangles) and PP1β-GFP (Fig. 5*G*, right graph, triangles) that were recruited to actin filaments by overexpression of SPECC1L-CT. Representative FRAP experiments for SPECC1L-GFP, Mypt1-GFP, and PP1β-GFP at actin filaments are show in Fig. S2*B*. It should be noted that PP1β did not show the same degree of reduced mobility as MYPT1 at the MT bundles and actin filaments. This is not unexpected, as it may be that SPECC1L and MYPT1 are more tightly associated with these structures while PP1β can still turn over on MYPT1 as it exchanges with other PP1 holoenzyme complexes.

While the recovery curves allow direct visual comparison by demonstrating the changes in turnover dynamics qualitatively, we quantitatively assessed these changes by calculating mobile fractions and recovery half-times. We were unable to fit single exponential recovery curves to the data, indicating the presence of more than one recovery pool. Double exponential curves provided a better fit in each case (R^2 values > 0.95). For all conditions, we determined the fraction that does not recover within 90 s post bleach (immobilized), the fraction that recovers with fast kinetics, and the fraction that recovers with slow kinetics. The half-times of recovery for the fast and slow pools were also determined. These values are summarized in Table S1, with the distribution of the GFP fusion proteins between immobile/slow/fast pools graphically represented in Fig. 5*H*. Taken together with the observed changes in subcellular distribution (Fig. 5, *A*–*E*), they show that SPECC1L has a profound effect on both the localization and turnover dynamics of MYPT1 and PP1β. These results suggest that SPECC1L can directly mediate the homeostatic distribution of MYPT1/PP1β between the MT and F-actin networks in interphase cells (Fig. 7*A*).

Association of SPECC1L with actin- and microtubule-related proteins is dynamic and changes throughout the cell cycle

Our MYPT1 and SPECC1L interactomes detected several actin-binding proteins that also associate with MTs and can regulate their stability. These include CAPZB, Coronin, and Spectrin family members (Fig. 1*E*; Supplemental Data File 1). The MT-associated proteins MAP1A/B and MAP4 were also detected but not as highly enriched (Supplemental Data File 1). When we used a BioID/MS approach to map the interactome of transiently overexpressed SPECC1L-BirA*, we saw a significant enrichment of MAP4 (Fig. 6*A*) that is consistent with its observed accumulation at SPECC1L-induced MT bundles (Fig. 4*E*). The MYPT1/PP1β complex was also highly enriched in the BioID dataset, along with several structure- and motility-related factors that include myosin (MYO1B), cortactin (CTTN), Coronin-1B (COROB1B), and the CRK-CRKL adaptor proteins that bridge tyrosine phosphorylation events to diverse intracellular signaling pathways (Supplemental Data File 2).

Having observed that removal of the C-terminal CH domain shifts the balance of steady-state SPECC1L association more

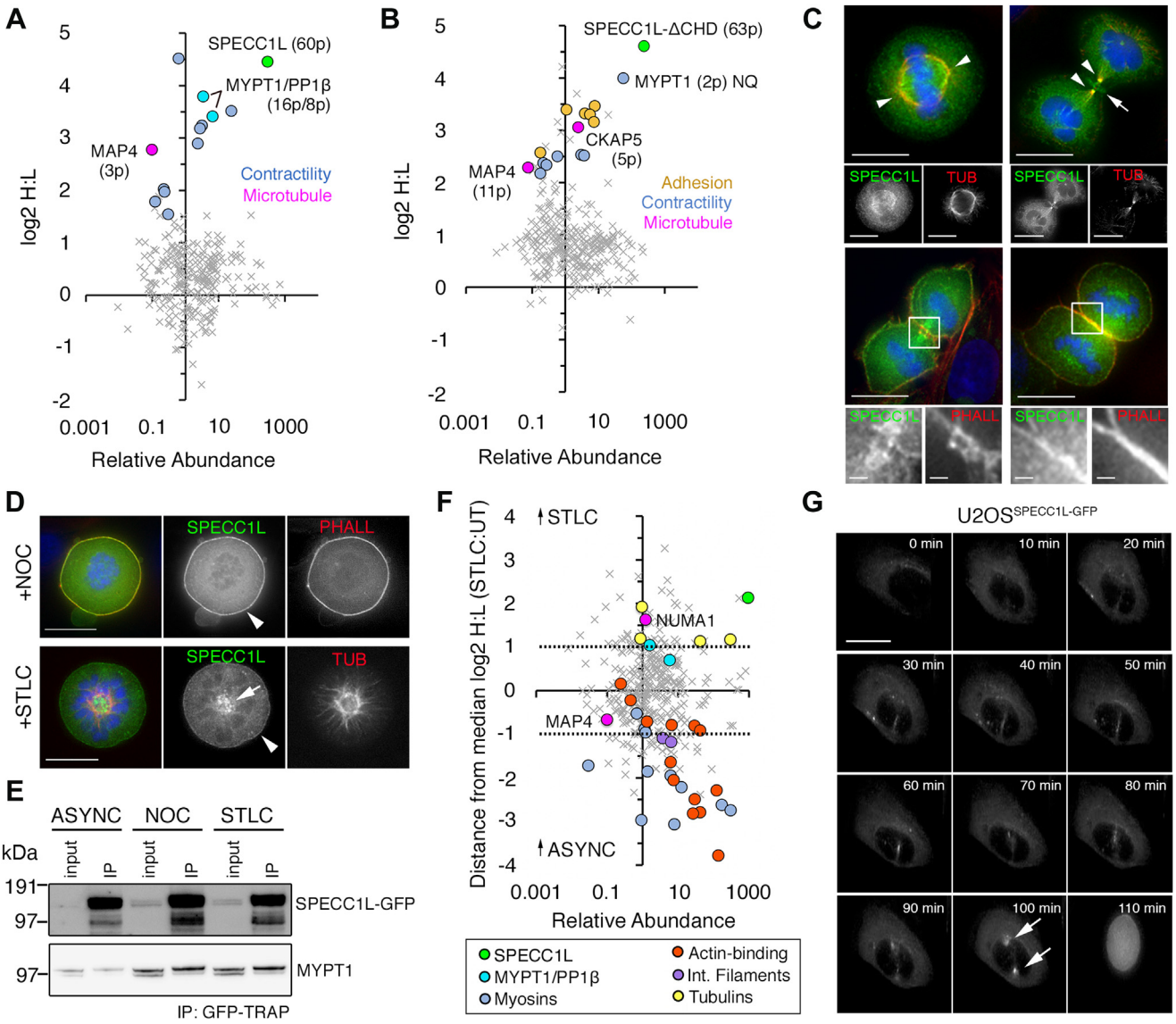

Figure 6. Association of SPECC1L with both microtubule and actin cytoskeletal proteins is dynamic and changes throughout the cell cycle. *A.* the graph shows proteins that are biotinylated by BirA*-tagged SPECC1L in a quantitative SILAC BioID/MS experiment. For the highlighted proteins, the number of peptides detected is indicated in parentheses. *B.* the graph shows proteins that are biotinylated by BirA*-tagged SPECC1L-ΔCHD in a quantitative SILAC BioID/MS experiment. For the highlighted proteins, the number of peptides detected is indicated in parentheses. As noted, MYPT1 was detected but not quantified (summed heavy:light peptide intensities were 47:1). The full BioID/MS datasets are provided in Supplemental Data File 2. *C.* the top panels show colocalization of SPECC1L (green) in the U2OS$^{SPECC1L\text{-}GFP}$ stable line with spindles (left, arrowheads in metaphase cell) and midbodies (right, arrowheads in telophase cell) visualized by anti-tubulin staining (*red*). Hoechst 33342-stained DNA is shown in *blue*. Additional accumulation between the midbodies was observed in telophase cells (*arrow*). The bottom panels show colocalization of SPECC1L (*green*) in the U2OS$^{SPECC1L\text{-}GFP}$ stable line at the cleavage furrow and the cortex with Phalloidin-stained actin filaments (*red*). Hoechst 33342-stained DNA is shown in *blue*. *D.* in nocodazole (NOC)-arrested U2OS$^{SPECC1L\text{-}GFP}$ cells, SPECC1L-GFP (*green*) is diffuse in the cytoplasm, remaining distinct from condensed chromosomes (*blue*) and showing additional accumulation with filamentous actin (Phalloidin, *red*) at the cell cortex. In STLC-arrested U2OS$^{SPECC1L\text{-}GFP}$ cells, SPECC1L-GFP (*green*) is diffuse in the cytoplasm, remaining distinct from condensed chromosomes (*blue*) and accumulating at the cortex and in the spindle pole region (*arrow*) at the center of the anti-tubulin stained monoastral spindle (*red*). *E.* immunoprecipitation/Western blot analysis confirmed association of MYPT1 with SPECC1L throughout the cell cycle. *F.* results of a quantitative SILAC AP/MS experiment comparing enrichment of interactors with SPECC1L-GFP immunoprecipitated from asynchronous U2OS$^{SPECC1L\text{-}GFP}$ cells (L) *versus* U2OS$^{SPECC1L\text{-}GFP}$ cells arrested at metaphase by overnight treatment with S-trityl-L-cysteine (STLC; H). Enrichment is expressed as the displacement from the median H:L ratio, with factors enriched <2-fold in either direction considered to bind equally under both conditions (area between the dashed lines). Interactors enriched >2-fold with SPECC1L-GFP from mitotic cell extracts are above the dashed line while interactors enriched >2-fold with SPECC1L-GFP from asynchronous cell extracts fall below the dashed line. The full AP/MS dataset is provided in Supplemental Data File 1. *G.* live imaging revealed transient association of SPECC1L-GFP with centrosomes (*arrows*) at the onset of mitosis. The scale bars represent 10 μm. AP/MS, affinity purification/mass spectrometry; SILAC, stable isotope labeling by amino acids in culture.

equally between MTs and actin filaments (Fig. 3*G*), we were interested to see how that was reflected in its proximity interactome. As shown in Fig. 6*B*, MAP4 is again enriched, along with the MT polymerase CKAP5 (49) (Fig. 6*B*). The Coronins CORO1B and CORO1C were also enriched, as were adhesion-related Syndecan family proteins (SDC1/2/4) that provide mechanical links between the extracellular matrix and the actin cytoskeleton.

Dynamic redistribution of SPECC1L between actin and tubulin structures is also observed in mitosis. Spindle association predominates during metaphase, with increased accumulation observed at the cleavage furrow during cytokinesis (Fig. 6*C*). We reasoned that this would be reflected in its interactome and quantitatively compared proteins enriched with SPECC1L-GFP (by SILAC AP/MS) from asynchronous U2OS$^{SPECC1L\text{-}GFP}$ cells (primarily interphase) *versus* U2OS$^{SPECC1L\text{-}GFP}$ cells arrested at metaphase by overnight treatment with the Eg5 inhibitor S-trityl-L-cysteine (STLC). In comparison with NOC-induced arrest, which destabilizes MTs and leaves SPECC1L diffuse in the cytoplasm and decorating the cell cortex, STLC-induced arrest stabilizes MTs in a monoaster spindle with which SPECC1L remains associated (Fig. 6*D*). The graph in Fig. 6*F* shows the distance from the median log2 H:L ratio for all identified proteins (*versus* their relative abundance in the AP), highlighting those were enriched >2-fold in either the Heavy (metaphase; above the top dashed line) or Light (interphase; below the bottom dashed line) condition. Proteins in the middle region between the two dashed lines were equally enriched in both conditions. Association of SPECC1L with MYPT1/PP1β persists throughout the cell cycle, which was also confirmed by IP/WB analysis (Fig. 6*E*).

Consistent with its change in localization, the majority of actomyosin-related proteins were enriched more with SPECC1L from asynchronous cell lysates, while STLC treatment led to an increased association with tubulin. The centrosomal NuMA (nuclear mitotic apparatus) protein, which interacts with MTs and plays a role in the formation and organization of the mitotic spindle, was also enriched with SPECC1L in STLC-arrested cells. Along with dynein, this protein is required to anchor minus-end MTs to centrosomes in mitosis (50) and promotes spindle bipolarity by organizing the radial array of MTs that incorporates Eg5 (51). SPECC1L-GFP in STLC-arrested cells does show a clustering at the center of the monoaster spindle (Fig. 6*D*) similar to that shown previously for NuMA (51, 52). This suggests that they associate at the spindle pole. Transient recruitment of SPECC1L to centrosomes had been previously noted but not shown. Long-term live imaging of our U2OS$^{SPECC1L\text{-}GFP}$ cell line confirmed enrichment of GFP-tagged Specc1L at centrosomes just prior to the onset of mitosis (Fig. 6*G*).

We further confirmed that, consistent with its association with the MT network during interphase (Fig. 3*A*), the N-terminal half of SPECC1L accumulates at the spindle in metaphase and anaphase and remains associated with the midbody in telophase (Fig. S3*A*). Similarly, the actin-associated C-terminal half of SPECC1L (Fig. 3*B*) is detected at the cell cortex in metaphase and shows localized accumulation at the cleavage furrow in anaphase and telophase (Fig. S3*B*).

Reasoning that posttranslational modifications such as reversible phosphorylation might mediate its subcellular redistribution, we quantified SPECC1L phosphopeptides detected in STLC-arrested *versus* asynchronous cells. The largest change was an increase in phospho-Ser1003 in STLC-arrested cells (log2 H:L = 4). This site lies just upstream of the CH domain. Although the introduction of either phosphomimic (S1003D) or nonphosphorylatable (S1003A) mutations in full-length SPECC1L or SPECC1L-CT had no detectable effect on association with actin filaments in interphase cells, an aberrant accumulation of cytoplasmic actin fibers was detected in metaphase cells expressing SPECC1L-CT/S1003A (Fig. S3*C*). A similar phenotype was observed with SPECC1L knockdown in U2OS cells (31), suggesting that this construct may be acting as a dominant-negative mutant.

Discussion

MP was one of the first Ser/Thr protein phosphatase complexes identified (53), and a wealth of literature over the past 3 decades has functionally dissected its critical role in the regulation of actomyosin contractility. Along the way, there has been a growing appreciation of its contribution to the regulation of other key cellular events, including cytoskeletal organization, adhesion, mitosis, and transcription (see (22) for review). Its interactors are found throughout the cell, but what remains unclear is how it balances these diverse functions (and its subcellular distribution) and adapts to physiological changes. As an example, an elegant study (24) identified HDAC6, which plays an important role in MT deacetylation, as a substrate for MYPT1/PP1β. Our data are consistent with their model, which suggests that the MP complex balances contractility and MT acetylation by associating either with actomyosin or MT substrates (Fig. 7*A*). What has remained to be answered is how MYPT1 is efficiently recruited to these substrates in the cell and what drives association with one over the other.

Our identification of a novel complex comprising Mypt1/PP1β and proteins capable of associating dynamically with both the MT and actin networks makes SPECC1L (and possibly SPECC1) an attractive candidate for the "missing link" that regulates the distribution of phosphatase activity between these 2 structures. We showed that SPECC1L associates with MTs and with F-actin *via* N-terminal and C-terminal regions, respectively, and that it directly binds MYPT1 in a stable complex that can be purified from cell extracts. We also showed significant overlap of their interaction profiles under steady-state conditions. Furthermore, we demonstrated that SPECC1L can regulate the subcellular localization and turnover dynamics of the MYPT1/PP1β complex in cells, pushing the balance more toward MTs (and a stabilized/bundled phenotype) or F-actin (and increased stress fibers). HDAC6 was detected in our SPECC1L AP/MS screen, albeit below the stringent enrichment threshold. The most highly enriched MT protein in our SPECC1L BioID experiments (both full-length and the ΔCHD mutant) was MAP4. MAP4 was also detected, albeit closer to threshold, in our MYPT1 and SPECC1L AP/MS datasets. Given that phosphorylation induces its detachment from MTs, which in turn are destabilized (54), our future work will explore the possibility that MAP4 is a substrate for MYPT1/PP1β targeted to MTs by SPECC1L.

An interesting observation was that the single CH domain of SPECC1L can mediate, at least in part, its association with

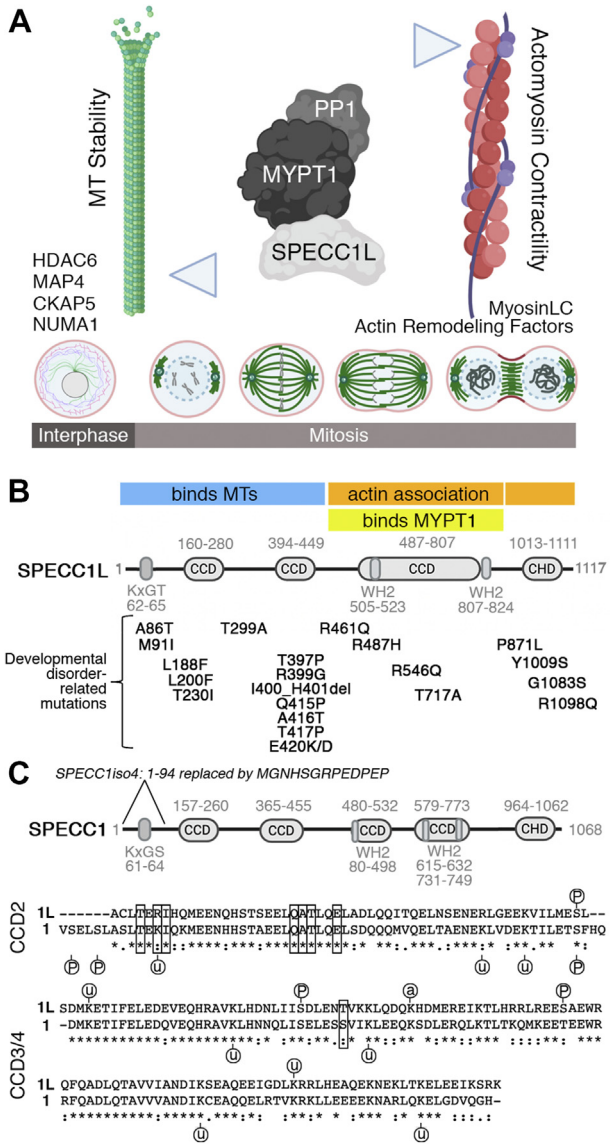

Figure 7. Location of disorder-related mutations within SPECC1L. *A.* proposed model in which SPECC1L regulates the balance of MYPT1/PP1β activity between microtubule (MT) and actomyosin-associated substrates throughout the cell cycle *via* direct binding to MYPT1. Putative microtubule- and actomyosin-associated factors enriched in our affinity purification/mass spectrometry and BioID datasets are noted. *B.* summary of SPECC1L mutations that have been linked to developmental defects. *C.* comparison of the regions that are most highly conserved regions between SPECC1L and SPECC1 in the CCD2 domain (>66% identical; aa 394–449 and 365–426 shown for SPECC1L and SPECC1, respectively) and the CCD3/4 domains (>60% identical, aa 684–799 and 660–773 shown for SPECC1L and SPECC1, respectively). Boxes highlight disorder-related mutations that are conserved, and posttranslational modifications (P, phosphorylation and u, ubiquitination) annotated on PhosphoSite Plus for both proteins are indicated.

actin, as 2 tandem CH domains are normally required for this interaction. A previous study noted that the CH domain in SPECC1L showed moderate homology to those found in α-actinin, Macrophin, Beta-Spectrin, and Smoothelin (31). Smoothelin-like protein SMTNL1, which is primarily expressed in smooth and striated muscle cells, has been shown to be a negative regulator of both MP activity (toward myosin light chain) and MYPT1 expression (55, 56). We saw no indication that overexpression of SPECC1L altered MYPT1 protein levels, but future work will address whether or not it can modulate MP activity. Given that knockdown of MYPT1 has been shown to induce stress fibers (57), it may be that the stress fibers induced by SPECC1L-CT overexpression contain inactive MYPT1/PP1β. Another obvious question is whether or not SPECC1L itself is a substrate for MP. To test this, we immunoprecipitated SPECC1L from cells overexpressing either tagged MYPT1 or tag alone and mapped a residue (S384) that showed decreased phosphorylation when MYPT1 was overexpressed. Although this site lies within the MT-binding N terminus of SPECC1L, S384A (non-phosphorylatable) or S384D (phosphomimic) mutants showed no obvious changes in MT localization or the stabilization/bundling phenotype. More work will be needed to dissect both the functional relevance of this phosphosite and whether or not it is directly regulated by MP. Similarly, the relevance of the mitotic phosphorylation site that we identified in C-terminal actin-binding region (S1003), and the patient-associated mutations found in both the C-terminal actin binding and N-terminal MT binding regions (Fig. 7*B*), needs to be addressed further using different approaches. A limitation of our work, and that of others, has been the reliance on exogenous overexpression of SPECC1L mutants. Future work will introduce these mutations directly into the endogenous protein using CRISPR/Cas9 gene editing (58).

Identification of NuMA in the SPECC1L mitotic interactome was consistent with the observed accumulation of SPECC1L at the spindle pole in STLC-treated cells. NuMA is a key factor in the formation and organization of the mitotic spindle (59). It is a structural hub that associates with both MTs and dynein (among other factors), and binding to dynein has been shown to drive spindle pole focusing and positioning. The dynein/dynactin plus end-directed motor protein complex has also been implicated in mediation of mitotic checkpoint silencing, *via* transportation of kinetochore checkpoint proteins toward the spindle poles (60). Interestingly, several dynactins were detected in our MYPT1, but not SPECC1L datasets. This could indicate either that their association represents a MYPT1 role that does not involve SPECC1L or that MYPT1 forms a tighter complex with them. NuMA was also enriched in our MYPT1 interactome, and both proteins were recently shown to be regulated at centrosomes by O-linked N-acetylglucosamine (O-GlcNAc) modification (61). It is tempting to speculate that SPECC1L, which we have shown to localize to centrosomes just prior to the onset of mitosis and accumulate at the pole following STLC arrest, also plays a role in the MYPT1-based regulation of spindle formation/maintenance. The specific enrichment of beta-tubulin with SPECC1L in STLC-arrested cells is also intriguing, as its phosphorylation by CDK1 impairs association with MTs (62). And, given the presence of both MYPT1 and SPECC1L at the cleavage furrow during cytokinesis, future work with synchronized cells will be needed to more comprehensively map their interactomes throughout the cell cycle.

Other outstanding questions include whether or not SPECC1L only binds MYPT1 that is in complex with PP1β and if their association is under some type of regulatory control.

Although we cannot determine stoichiometry from our AP/MS datasets, our observation that overexpressed MYPT1 copurified with only PP1β (detected with a similar relative abundance) and SPECC1L (at a lower abundance) suggests that SPECC1L associates with a subset of MYPT1/PP1β dimers to form a trimeric complex. And, although we demonstrated that their association persists throughout the cell cycle, that does not rule out a signaling event that controls their binding in a spatial and/or temporal manner. Having mapped the MYPT1 interaction domain on SPECC1L to a region containing the third CCD, we compared its sequence with that of the related region in SPECC1 (CCD4) and identified a stretch of ∼120 residues with >60% identity (*versus* 42.5% overall identity for the full-length proteins; Fig. 7*C*). Future work will determine if this is the minimal domain required for binding MYPT1 and, if so, whether or not it contains any sites that are subject to regulated PTMs that can impact binding affinity. The Thr residue in the developmental disorder–related patient mutation that falls within this region, T717A, is a Ser residue in SPECC1 and thus may be subject to phosphoregulation by a Ser/Thr protein kinase. In addition, known PTMs annotated for SPECC1L and SPECC1 by PhosphoSite Plus are on conserved residues (Fig. 7*C*).

Our work has identified a previously unknown direct interaction of SPECC1L/1 with MYPT1, which can impact the subcellular localization and activity of the MYPT1/PP1β complex. Further characterization of the functional significance of this regulation will be necessary to evaluate its potential as a therapeutic target.

Experimental PROCEDURES

Plasmids and antibodies

Full-length MYPT1 and MYPT1 fragments were amplified from cDNA (Open BioSystems) using specific primers and inserted into the pEGFP/mCherry(C1), pEGFP(N3), and pGEX-4-T3 vectors by restriction cloning. Full-length SPECC1L, SPECC1/iso1, and SPECC1/iso4 (and their respective fragments) were inserted into pEGFP(C1), pEGFP(N3), pET-47b(+) and myc-BirA*(C1) and HA-BirA*(N3) vectors using the same approach. The phosphorylation mutants were generated using QuickChange mutagenesis (Agilent). All cloning was confirmed by DNA sequencing (StemCore Laboratories, Ottawa Hospital Research Institute). The pEGFP(N3)-PP1β plasmid was previously described (63) and is available through Addgene (plasmid #44223).

Anti-MYPT1 antibodies were obtained from Bethyl Laboratories; anti-SPECC1L(CYTSA) antibodies from ProteinTech; and anti-alpha-tubulin, anti-acetylated(K40)-alpha-tubulin, and anti-GFP antibodies from Millipore Sigma. The PP1β antibody was previously described (64). All HRP- and fluorophore-conjugated secondary antibodies and streptavidin were from ThermoFisher.

Cell culture

U2OS cells were obtained from ATCC and grown in Dulbecco's modified Eagles' medium (DMEM) supplemented with 10% fetal calf serum and 100 U/ml penicillin and streptomycin (Wisent Bioproducts Inc). Stable cell lines were generated as described and maintained in media supplemented with G418 (65). The mouse Mypt1-GFP bacterial artificial chromosome HeLa cell line was a gift from Dr Tony Hyman (MPI-CBG, Germany) (48). Cells were transfected with either 1 mg/ml polyethylenimine (Polysciences, Inc.) or Effectene transfection reagent (Qiagen). For mitotic arrest experiments, cells were treated with either 3.3 μM nocodazole (NOC) or 5 μM S-trityl-L-cysteine (STLC) for 18 h. For short-term MT destabilization and disruption of actin polymerization, cells were treated with either 8.3 uM nocodazole (NOC) or 2 uM Latrunculin (LAT) for 2 h, respectively.

Metabolic labeling

Stable isotope labeling with amino acids in cell culture (SILAC) for label-based quantitative MS was carried out as described (33). Briefly, cells were grown for 7 to 10 passages in high-glucose DMEM containing either L-arginine and L-lysine (Light) or the isotopes L-arginine13C/15N and L-lysine13C/15N (Heavy). SILAC media was prepared by supplementing high-glucose DMEM minus Arg/Lys/Leu/Met (AthenaES) with 10% dialyzed FBS (ThermoFisher) and the appropriate amino acids, mixing well and filtering through a 0.22-μm filter (Millipore). For the SPECC1L metaphase arrest *versus* asynchronous AP/MS experiment, Light isotope-encoded U2OS$^{S\text{-}PECC1L\text{-}GFP}$ were left untreated for standard harvesting while Heavy-isotope encoded U2OS$^{SPECC1L\text{-}GFP}$ cells were treated for 18 h with STLC and harvested by mitotic shake-off. For the BioID experiments, Heavy isotope-encoded cells were transfected with BirA*-SPECC1L constructs and Light isotope-encoded cells with the respective GFP-tagged constructs, and the medium was supplemented with 50 μM biotin for 18 h.

Preparation of cell extracts and affinity purification

For standard WB and AP/MS experiments, whole cell extracts were prepared by scraping cells into ice-cold RIPA buffer (50 mM Tris pH 7.5, 150 mM NaCl, 1% NP-40, 0.5% deoxycholate, protease inhibitors), sonicating and clearing by centrifuging at 2800*g* for 10 min at 4 °C. For BioID experiments, whole cell extracts were prepared in a similar fashion, but the salt concentration in the RIPA was increased to 500 mM.

To increase interactome coverage in the MYPT1 and SPECC1L-GFP AP/MS experiments, separate cytoplasmic and nuclear fractions were prepared for the AP/MS steps and the MS results concatenated at the analysis step (66). All solutions used in the fractionation, extraction, and AP protocols are supplemented with EDTA-free COMPLETE protease inhibitors (Millipore Sigma) to minimize protein degradation. Total protein concentrations for all extracts were measured using a Bradford assay.

For capture of endogenous MYPT1 from cell extracts, MYPT1 antibody (Bethyl Lab) was covalently conjugated to protein A Dynabeads (Invitrogen). Covalently conjugated affinity purified IgG from the same species (Rabbit;

ThermoFisher) was used for the control AP. For capture of GFP-tagged proteins from cell extracts, an equal amount of total protein extract for each condition was incubated with GFP-Trap_A beads (Chromotek) at 4 °C for 1 h. Post AP, the affinity matrices were washed 3× with RIPA buffer and bound proteins eluted with a bead equivalent volume of 1% SDS.

For the BioID experiments, the salt concentration in the lysates was first reduced to 250 mM by adding an equal volume of RIPA buffer with 0 mM NaCl. Equal amounts of total protein extract for each condition were incubated with Streptavidin-agarose beads (ThermoFisher) at 4 °C for 4 h and bound proteins eluted with 2% SDS/30 mM biotin.

For immunoblotting, LDS sample buffer (Invitrogen) was added to lysates and bead eluents and the proteins resolved on a 4 to 12% Novex Nu-PAGE bis-Tris polyacrylamide gel (ThermoFisher) and transferred to nitrocellulose membranes. For the SILAC AP/MS and SILAC BioID/MS experiments, beads from the different conditions were combined prior to the elution step, to minimize variability in downstream processing. The eluted proteins were then reduced and alkylated by treatment with DTT and iodoacetamide, respectively. Sample buffer was added, and the proteins were resolved by electrophoresis on a NuPAGE 10% BisTris gel (ThermoFisher). The gel was stained using SimplyBlue Safestain (ThermoFisher) and the entire lane cut into five slices. Each slice was cut into 2 × 2 mm fragments, destained, and digested overnight at 30 °C with Trypsin Gold (ThermoFisher).

Mass spectrometry and data analysis

An aliquot of each tryptic digest was analyzed by liquid chromatography–tandem mass spectrometry on an Orbitrap Fusion Lumos system (Thermo Scientific) coupled to a Dionex UltiMate 3000 RSLC nano HPL. The raw files were searched against the Human UniProt Database using MaxQuant software v1.5.5.1 (http://www.maxquant.org) (67) and the following criteria: peptide tolerance = 10 ppm, trypsin as the enzyme (2 missed cleavages allowed), and carboxyamidomethylation of cysteine as a fixed modification. Variable modifications are oxidation of methionine and N-terminal acetylation. Heavy SILAC labels were Arg10 (R10) and Lys8 (K8). Quantitation of SILAC ratios was based on razor and unique peptides, and the minimum ratio count was 2. The peptide and protein FDR was 0.01. The AP/MS and BioID datasets (minus common environmental contaminants as per http://maxquant.org and proteins identified *via* the decoy database) are provided in the Supplemental Data Files.

Fluorescence microscopy

Cells seeded on No. 1.5 coverslips were fixed for 10 min at 37 °C in 3.7% (wt/vol) paraformaldehyde (PFA) in PHEM buffer (60 mM Pipes pH 6.8, 27 mM Hepes, 20 mM EGTA, 16 mM $MgSO_4$, pH 7.0 with 10 M KOH). Following a 10-min permeabilization with 1% Triton X-100 in PBS, nonspecific binding sites were blocked by incubation in PBS with 0.2% Tween-20 and either 1% donkey serum (for immunostaining) or 1% BSA (for Streptavidin staining of biotinylated proteins). For immunostaining, cells were incubated with the appropriate primary antibody, followed by incubation with the appropriate fluorophore-conjugated secondary antibody. Coverslips were prepared for imaging by mounting in Vectashield liquid mounting media (Vector Labs). For BioID, cells were incubated with fluorophore-tagged Streptavidin (ThermoFisher).

For live imaging, cells were cultured in 35-μm optically clear polymer-bottom u-dishes (ibidi) and growth medium was replaced with Phenol Red–free CO_2-independent medium (ThermoFisher). If desired, DNA was stained by incubating the cells for 20 min at 37 °C in medium containing 0.25 μg/ml Hoechst No. 33342 (Millipore Sigma). Images were acquired using a DeltaVision CORE widefield fluorescence system fitted with a 60 × NA 1.4 PlanApochromat objective (Olympus), CoolSNAP charge-coupled device camera (Roper Scientific) and environmental chamber. The microscope was controlled and images were processed by SoftWorX acquisition and deconvolution software (GE Healthcare). All images are single, deconvolved optical sections.

Photobleaching experiments were carried out as described (68). Briefly, cells were cultured in glass-bottom dishes (Ted Pella). Three single sections were imaged before photobleaching, an ROI was then bleached to ∼50% of its original intensity using the 488-nm laser, and a rapid series of images was acquired after the photobleaching period for a total of 90 s. Recovery curves were plotted and the mobile fractions and half-times of recovery determined using GraphPad Prism.

Super-resolution imaging

Expansion microscopy–based super-resolution imaging was carried out as per our modification (46) of the X10 protocol (45). Briefly, cells seeded on coverslips were transfected for 18 h to drive transient overexpression of SPECC1L-GFP. They were then PFA-fixed and permeabilized, and stained with anti-acetylated-alpha-tubulin and anti-mouse-Alexa647. To counteract the reduction in GFP signal following expansion, cells were also stained with rabbit anti-GFP and anti-rabbit-Alexa 488 antibodies. The stained cells were then incubated overnight at room temperature with Acryloyl-X anchoring reagent (ThermoFisher). The gelation solution was prepared by mixing 1.335 g DMAA and 0.32 g sodium acrylate (Millipore Sigma) with 2.85 g ddH_2O, vortexing and purging O_2 by bubbling with N_2 for 40 min at room temperature. A solution of 0.036 g/ml of potassium persulfate was prepared in ddH2O, 0.3 ml added to 2.7 ml of gelation solution and O_2 purged by bubbling with N_2 for 15 min on ice. Gelation chambers were prepared by sandwiching the stained coverslip, cell side up, between 2 coverslips and adding spacer coverslips along the sides. TEMED was added to the gelation mix, 100 μl of the solution was pipetted on top of the cells using a prechilled pipette tip, and a 22 × 22 mm coverslip was placed on top. Gels were placed in a humidified chamber and allowed to polymerize for 3 h at room temperature. The gels were removed from the coverslips and incubated overnight at 50 °C with 8 U/ml Proteinase K (Sigma-Aldrich) prepared fresh in digestion buffer (50 mM Tris, 800 mM Guanidine HCl, 1 mM EDTA,

and 0.5% (v/v) Triton X-100 in ddH2O, pH 8.0). To swell the gels, deionized water containing 1.7 μg/ml Hoechst 33342 was added. After 10 min, this was replaced with two more washes of deionized water for a total of 1 h expansion. To image cells post expansion, segments were removed using a custom 3D-printer gel cutter (46) and transferred to 8-well chambered coverslips (ibidi). Multiwavelength Z-stacks were acquired using a Zeiss LSM880 confocal laser scanning microscope with a 63×/1.4 NA Plan-Apo objective in AiryScan mode.

For direct stochastic optical reconstruction microscopy super-resolution imaging, cells seeded on No 1.5 coverslips were transfected for 18 h to drive transient overexpression of Specc1L-GFP, and then PFA-fixed, permeabilized, and stained with anti-acetylated-alpha-tubulin and anti-mouse-Alexa 647. The coverslips were mounted in a 40% Vectashield, 60% Tris/glycerol solution that has been shown to support efficient blinking of Alexa 647 (69). Images were acquired on a Quorum spinning disk confocal system (Quorum Technologies) using a 63×/1.4NA objective, a Hamamatsu EM-charge-coupled device ImagEM camera, and the appropriate laser lines and filter sets. Initially, widefield and spinning disk confocal images were acquired for both the SPECC1L-GFP signal (490 nm laser and FITC emission filter set) and the anti-acetylated-alpha-tubulin-Alexa 647 signal (639-nm laser and Cy5 emission filter set) using low laser power. An ROI was then chosen for super-resolution imaging, using the MetaMorph Single Molecule Resolution real-time acquisition and analysis module (Molecular Devices LLC). Stochastic activation of the Alexa 647 fluorophores was achieved by firing the 639-nm laser at full power, which causes them to blink as they cycled through their ON/OFF states. A series of 10,000 images was acquired, and a super-resolved image was reconstructed from the individual x-y localizations mapped in each image.

Purification of recombinant proteins for in vitro *assays*

Plasmids expressing recombinant 6× His-tagged SPECC1L fragments were transformed in BL-21 cells and plated on LB/ampicillin plates overnight at 37 °C. LB was inoculated with a colony and expanded to a larger culture that was induced with 0.5 mM IPTG once the A_{600} reached ∼0.5. Following 18 h incubation at 16 °C, the culture was pelleted, resuspended in buffer (20 mM Tris pH 7.5, 250 mM NaCl, 10 mM Imidazole) containing 1 mg/ml of Lysozyme, and incubated on ice for 30 min. Following sonication and pelleting of cell debris, the lysate was incubated with Ni^{2+}-NTA agarose beads (Qiagen) at 4 °C for 1 h with end-over-end rotation. The beads were pelleted and washed 3× with wash buffer (20 mM Tris pH7.5, 0.5 M NaCl, and 20 mM Imidazole). The His-tagged proteins were eluted with elution buffer (20 mM Tris pH7.5, 0.5 M NaCl, and 300 mM Imidazole) at 500-μl increments and dialyzed in TGEM buffer (20 mM Tris-HCl pH7.9, 0.1 M NaCl, 20% glycerol, 1 mM EDTA, 5 mM $MgCl_2$, 0.1% NP-40, 0.2 mM PMSF). After dialysis 1 mM DTT was added prior to use in the *in vitro* assays.

Plasmids expressing recombinant GST-tagged Mypt1(CD) or GST alone were transformed in Rosetta cells and plated on LB/ampicillin plates overnight at 37 °C. LB was inoculated with a colony and expanded to larger culture that was induced with 0.2 mM-0.5 mM IPTG once the A_{600} reached ∼0.5. Following 18 h incubation at 16 °C, the culture was pelleted and resuspended in buffer (50 mM Tris pH 8.0, 2 mM EDTA pH 8.0, 0.1% BME, and protease inhibitor). Following sonication and pelleting of cell debris, NaCl was added to a final concentration of 0.25 M and the lysate was incubated with Glutathione sepharose beads (GE Healthcare) at 4 °C for 1 h with end-over-end rotation. The beads were pelleted and washed 3× with wash buffer (20 mM Tris pH7.5, 0.25 M NaCl, 2 mM EDTA, 2 mM EGTA). GST-Mypt1(CD) was eluted using 10 ml wash buffer containing 61 mg of reduced glutathione and 13 μl of 10 M NaOH (pH 8.0). The eluted protein was dialyzed in TGEM buffer (20 mM Tris-HCl pH 7.9, 0.1 M NaCl, 20% glycerol, 1 mM EDTA, 5 mM $MgCl_2$, 0.1% NP-40, 0.2 mM PMSF). After dialysis 1 mM DTT was added prior to use in the *in vitro* assays.

In vitro *coimmunoprecipitation assay*

Purified recombinant HisSpecc1LΔCD was combined with either GST and GST-Mypt1(CD) immobilized on Glutathione agarose beads. Following 1 h incubation at 4 °C, bound protein was eluted, subjected to SDS-PAGE, and transferred to nitrocellulose membrane for immunoblotting with anti-His and anti-mouse-HRP to detect the Specc1L fragment. The blot was then stripped and probed with anti-GST and anti-mouse-HRP.

Far western blot assay

Purified recombinant HisSpecc1LΔCD (6 μg) was separated by SDS-PAGE and transferred to nitrocellulose membrane. The membrane was incubated overnight with 10% milk (in PBS + 0.5% Tween) to block nonspecific binding sites and washed 3× with PBS/0.5%Tween, then 1× with PBS, before it was overlaid with 5 μg purified recombinant GST-Mypt (CD) or GST in 5 ml of 1 mg/ml BSA/PBS solution. The blot was then probed with anti-GST and anti-mouse HRP.

Microtubule-binding protein spin-down assay

The Microtubule Binding Protein Spin-Down assay was performed according to the manufacturers' protocol (Cytoskeleton). Briefly, stabilized MTs were prepared by incubating a 20-μl aliquot of Tubulin protein (5 mg/ml) at 35 °C with 2 μl of Cushion Buffer (80 mM Pipes pH7.0, 1 mM MgCl2, 1 mM EGTA, 60 % glycerol) for 20 min on ice. A volume of 2 μl of 2 mM Taxol was added to 200 μl of preheated (at 35 °C) General Tubulin Buffer (80 mM Pipes pH 7.0, 2 mM MgCl2, 0.5 mM EGTA), which was immediately added to the MTs after the 20-min incubation on ice. The sample was gently and thoroughly mixed and left at room temperature, allowing the MTs to stabilize. A volume of 20 μl of the stable MTs was then mixed with BSA, MAP4, or His-SPECC1L-NT (2–5 μg). After a 30-min incubation the samples were carefully pipetted onto 100 μl of Cushion Buffer (1 ml containing 10 μl of 2 mM Taxol) and centrifuged at 100,000*g* at room temperature for

40 min. The uppermost supernatant layer (50 µl) was removed and added to 16.7 µl of 4× Laemmli sample buffer. The remaining supernatant was discarded. The pellet was resuspended in 66.7 µl of 1× Laemmli sample buffer. A volume of 20 µl of the supernatant and pellet sample were subjected to SDS-PAGE and either Coomassie stained or transferred to nitrocellulose for immunoblotting.

Actin fractionation assay

U2OS cells cotransfected with Flag-tagged Actin (wildtype or R62D nonpolymerizable mutant) and GFP-tagged constructs were washed in PBS and extracted with 0. 5 ml of cytoskeletal buffer (50 mM MES pH 6.8, 1 mM EGTA, 50 mM KCl, 1 mM MgCl2, 0.5% Triton X-100, protease inhibitors) on a shaking incubator. After 2 min, the Triton X-100-soluble fraction was removed and the Triton X-100 insoluble fraction was scraped off the dishes into 0.5 ml of the same buffer and sonicated. Aliquots of each fraction (100 µl) were mixed with equivalent amount of LDS sample buffer and reduced to a final volume of 45 µl in a SpeedVac for separation by 10% SDS-PAGE, transfer to nitrocellulose, and immunoblot analysis using anti-Flag and anti-GFP antibodies.

Data availability

All proteomic datasets are included as Supporting Information.

Supporting information—This article contains supporting information.

Acknowledgments—We thank colleagues in the Trinkle-Mulcahy lab for helpful discussions and suggestions and Priyam Maini for technical contributions. We also thank Drs. Ina Poser and Anthony Hyman for reagents and Lawrence Puente at the Ottawa Hospital Research Institute Proteomics Core Facility for technical support. We acknowledge the outstanding support of the Cell Biology and Image Acquisition Core (RRID: SCR_021845) funded by the University of Ottawa and the Canada Foundation for Innovation.

Author contributions—V. M., J. W. C., L. T.-M. conceptualization; V. M., S. O., L. T.-M. methodology; S. O. validation; V. M., N. D., A. G.-L. investigation; V. M. writing – original draft; J. W. C., L. T.-M. writing – review & editing; V. M., L. T.-M. visualization; L. T.-M. supervision; L. T.-M. funding acquisition.

Funding and additional information—This work was supported by Natural Sciences and Engineering Research Council Discovery Grants 06674 and 5018217 (to L.T.-M.) and a Canadian Institutes of Health Research Banting & Best Scholarship (to V.M.).

Conflict of interest—The authors declare that they have no conflicts of interest with the contents of this article.

Abbreviations—The abbreviations used are: AP/MS, affinity purification/mass spectrometry; BSA, bovine serum albumin; DMEM, Dulbecco's modified Eagle's medium; FRAP, fluorescence recovery after photobleaching; IP, immunoprecipitation; MP, myosin phosphatase; MT, microtubule; NOC, nocodazole; PFA, paraformaldehyde; PP1, protein phosphatase 1; $PP1_{cat}$, PP1 catalytic subunit; PTM, post-translational modification; ROI, region of interest; SILAC, stable isotope labeling by amino acids in culture; STLC, S-trityl-L-cysteine; WB, Western blot.

References

1. Olsen, J. V., Blagoev, B., Gnad, F., Macek, B., Kumar, C., Mortensen, P., *et al.* (2006) Global, in vivo, and site-specific phosphorylation dynamics in signaling networks. *Cell* **127**, 635–648
2. Venerando, A., Cesaro, L., and Pinna, L. A. (2017) From phosphoproteins to phosphoproteomes: A historical account. *FEBS J.* **284**, 1936–1951
3. Roadcap, D. W., Brush, M. H., and Shenolikar, S. (2007) Identification of cellular protein phosphatase-1 regulators. *Methods Mol. Biol.* **365**, 181–196
4. Korrodi-Gregório, L., Esteves, S. L. C., and Fardilha, M. (2014) Protein phosphatase 1 catalytic isoforms: Specificity toward interacting proteins. *Transl Res.* **164**, 366–391
5. Cohen, P. T. W. (2002) Protein phosphatase 1–targeted in many directions. *J. Cell. Sci.* **115**(Pt 2), 241–256
6. Heroes, E., Lesage, B., Görnemann, J., Beullens, M., Van Meervelt, L., and Bollen, M. (2013) The PP1 binding code: A molecular-lego strategy that governs specificity. *FEBS J.* **280**, 584–595
7. Trinkle-Mulcahy, L., Andersen, J., Lam, Y. W., Moorhead, G., Mann, M., and Lamond, A. I. (2006) Repo-Man recruits PP1 gamma to chromatin and is essential for cell viability. *J. Cell Biol.* **172**, 679–692
8. Moorhead, G. B. G., Trinkle-Mulcahy, L., Nimick, M., De Wever, V., Campbell, D. G., Gourlay, R., *et al.* (2008) Displacement affinity chromatography of protein phosphatase one (PP1) complexes. *BMC Biochem.* **9**, 1–10
9. Chamousset, D., De Wever, V., Moorhead, G. B., Chen, Y., Boisvert, F.-M., Lamond, A. I., *et al.* (2010) RRP1B targets PP1 to mammalian cell nucleoli and is associated with Pre-60S ribosomal subunits. *Mol. Biol. Cell* **21**, 4212–4226
10. Bennett, D., Lyulcheva, E., Alphey, L., and Hawcroft, G. (2006) Towards a comprehensive analysis of the protein phosphatase 1 interactome in Drosophila. *J. Mol. Biol.* **364**, 196–212
11. Fardilha, M., Esteves, S. L. C., Korrodi-Gregório, L., Vintém, A. P., Domingues, S. C., Rebelo, S., *et al.* (2011) Identification of the human testis protein phosphatase 1 interactome. *Biochem. Pharmacol.* **82**, 1403–1415
12. Flores-Delgado, G., Liu, C. W. Y., Sposto, R., and Berndt, N. (2007) A limited screen for protein interactions reveals new roles for protein phosphatase 1 in cell cycle control and apoptosis. *J. Proteome Res.* **6**, 1165–1175
13. Yadav, L., Tamene, F., Göös, H., van Drogen, A., Katainen, R., Aebersold, R., *et al.* (2017) Systematic analysis of human protein phosphatase interactions and dynamics. *Cell Syst* **4**, 430–444.e5
14. Egloff, M. P., Johnson, D. F., Moorhead, G., Cohen, P. T., Cohen, P., and Barford, D. (1997) Structural basis for the recognition of regulatory subunits by the catalytic subunit of protein phosphatase 1. *EMBO J.* **16**, 1876–1887
15. Bollen, M., Peti, W., Ragusa, M. J., and Beullens, M. (2010) The extended PP1 toolkit: Designed to create specificity. *Trends Biochem. Sci.* **35**, 450–458
16. Brozovich, F. V. (2002) Myosin light chain phosphatase. *Circ. Res.* **90**, 500–502
17. Feng, J., Ito, M., Ichikawa, K., Isaka, N., Nishikawa, M., Hartshorne, D. J., *et al.* (1999) Inhibitory phosphorylation site for rho-associated kinase on smooth muscle myosin phosphatase*. *J. Biol. Chem.* **274**, 37385–37390
18. Aggen, J. B., Nairn, A. C., and Chamberlin, R. (2000) Regulation of protein phosphatase-1. *Chem. Biol.* **7**, R13–R23
19. Okamoto, R., Ito, M., Suzuki, N., Kongo, M., Moriki, N., Saito, H., *et al.* (2005) The targeted disruption of the MYPT1 gene results in embryonic lethality. *Transgenic Res.* **14**, 337–340
20. Virshup, D. M., and Shenolikar, S. (2009) From promiscuity to precision: Protein phosphatases get a makeover. *Mol. Cell* **33**, 537–545
21. Xia, D., Stull, J. T., and Kamm, K. E. (2005) Myosin phosphatase targeting subunit 1 affects cell migration by regulating myosin phosphorylation and actin assembly. *Exp. Cell Res.* **304**, 506–517

22. Kiss, A., Erdődi, F., and Lontay, B. (2019) Myosin phosphatase: unexpected functions of a long-known enzyme. *Biochim. Biophys. Acta Mol. Cell Res* **1866**, 2–15
23. Yamashiro, S., Yamakita, Y., Totsukawa, G., Goto, H., Kaibuchi, K., Ito, M., *et al.* (2008) Myosin phosphatase-targeting subunit 1 regulates mitosis by antagonizing polo-like kinase 1. *Dev. Cell* **14**, 787–797
24. Joo, E. E., and Yamada, K. M. (2014) MYPT1 regulates contractility and microtubule acetylation to modulate integrin adhesions and matrix assembly. *Nat. Commun.* **5**, 1–13
25. Saadi, I., Alkuraya, F. S., Gisselbrecht, S. S., Goessling, W., Cavallesco, R., Turbe-Doan, A., *et al.* (2011) Deficiency of the cytoskeletal protein SPECC1L leads to oblique facial clefting. *Am. J. Hum. Genet.* **89**, 44–55
26. Fan, F., Roszik, J., Xia, L., Ghosh, S., Wang, R., Ye, X., *et al.* (2022) Cytospin-A regulates colorectal cancer cell division and migration by modulating stability of microtubules and actin filaments. *Cancers (Basel)* **14**, 1–17
27. Kruszka, P., Li, D., Harr, M. H., Wilson, N. R., Swarr, D., McCormick, E. M., *et al.* (2015) Mutations in SPECC1L, encoding sperm antigen with calponin homology and coiled-coil domains 1-like, are found in some cases of autosomal dominant Opitz G/BBB syndrome. *J. Med. Genet.* **52**, 104–110
28. Bhoj, E. J., Haye, D., Toutain, A., Bonneau, D., Nielsen, I. K., Lund, I. B., *et al.* (2019) Phenotypic spectrum associated with SPECC1L pathogenic variants: New families and critical review of the nosology of Teebi, Opitz GBBB, and baraitser-winter syndromes. *Eur. J. Med. Genet.* **62**, 1–8
29. Zhang, T., Wu, Q., Zhu, L., Wu, D., Yang, R., Qi, M., *et al.* (2020) A novel SPECC1L mutation causing Teebi hypertelorism syndrome: expanding phenotypic and genetic spectrum. *Eur. J. Med. Genet.* **63**, 1–5
30. Migliore, C., Vendramin, A., McKee, S., Prontera, P., Faravelli, F., Sachdev, R., *et al.* (2022) SPECC1L mutations are not common in sporadic cases of Opitz G/BBB syndrome. *Genes (Basel)* **13**, 1–10
31. Mattison, C. P., Stumpff, J., Wordeman, L., and Winey, M. (2011) Mip1 associates with both the Mps1 kinase and actin, and is required for cell cortex stability and anaphase spindle positioning. *Cell Cycle* **10**, 783–793
32. Gimona, M., Djinovic-Carugo, K., Kranewitter, W. J., and Winder, S. J. (2002) Functional plasticity of CH domains. *FEBS Lett.* **513**, 98–106
33. Trinkle-Mulcahy, L., Boulon, S., Lam, Y. W., Urcia, R., Boisvert, F.-M., Vandermoere, F., *et al.* (2008) Identifying specific protein interaction partners using quantitative mass spectrometry and bead proteomes. *J. Cell Biol.* **183**, 223–239
34. Trinkle-Mulcahy, L. (2012) Resolving protein interactions and complexes by affinity purification followed by label-based quantitative mass spectrometry. *Proteomics* **12**, 1623–1638
35. Trinkle-Mulcahy, L. (2019) Recent advances in proximity-based labeling methods for interactome mapping. *F1000Res* **8**. https://doi.org/10.12688/f1000research.16903.1
36. Ashburner, M., Ball, C. A., Blake, J. A., Botstein, D., Butler, H., Cherry, J. M., *et al.* (2000) Gene Ontology: Tool for the unification of biology. *Nat. Genet.* **25**, 25–29
37. Linding, R., Russell, R. B., Neduva, V., and Gibson, T. J. (2003) GlobPlot: Exploring protein sequences for globularity and disorder. *Nucleic Acids Res.* **31**, 3701–3708
38. Wu, Y., Murányi, A., Erdodi, F., and Hartshorne, D. J. (2005) Localization of myosin phosphatase target subunit and its mutants. *J. Muscle Res. Cell Motil* **26**, 123–134
39. Kumar, M., Michael, S., Alvarado-Valverde, J., Mészáros, B., Sámano-Sánchez, H., Zeke, A., *et al.* (2022) The eukaryotic linear motif resource: 2022 release. *Nucleic Acids Res.* **50**, D497–D508
40. Lyubimova, A., Bershadsky, A. D., and Ben-Ze'ev, A. (1997) Autoregulation of actin synthesis responds to monomeric actin levels. *J. Cell Biochem.* **65**, 469–478
41. Posern, G., Sotiropoulos, A., and Treisman, R. (2002) Mutant actins demonstrate a role for unpolymerized actin in control of transcription by serum response factor. *MBoC* **13**, 4167–4178
42. Goering, J. P., Wenger, L. W., Stetsiv, M., Moedritzer, M., Hall, E. G., Isai, D. G., *et al.* (2021) In-frame deletion of SPECC1L microtubule association domain results in gain-of-function phenotypes affecting embryonic tissue movement and fusion events. *Hum. Mol. Genet.* **31**, 18–31
43. Magiera, M. M., Singh, P., Gadadhar, S., and Janke, C. (2018) Tubulin posttranslational modifications and emerging links to human disease. *Cell* **173**, 1323–1327
44. Shigematsu, H., Imasaki, T., Doki, C., Sumi, T., Aoki, M., Uchikubo-Kamo, T., *et al.* (2018) Structural insight into microtubule stabilization and kinesin inhibition by Tau family MAPs. *J. Cell Biol.* **217**, 4155–4163
45. Truckenbrodt, S., Maidorn, M., Crzan, D., Wildhagen, H., Kabatas, S., and Rizzoli, S. O. (2018) X10 expansion microscopy enables 25-nm resolution on conventional microscopes. *EMBO Rep.* **19**, e45836
46. Gaudreau-Lapierre, A., Mulatz, K., Béïque, J.-C., and Trinkle-Mulcahy, L. (2021) Expansion microscopy-based imaging of nuclear structures in cultured cells. *STAR Protoc.* **2**, 100630
47. van de Linde, S., Löschberger, A., Klein, T., Heidbreder, M., Wolter, S., Heilemann, M., *et al.* (2011) Direct stochastic optical reconstruction microscopy with standard fluorescent probes. *Nat. Protoc.* **6**, 991–1009
48. Poser, I., Sarov, M., Hutchins, J. R. A., Hériché, J.-K., Toyoda, Y., Pozniakovsky, A., *et al.* (2008) BAC TransgeneOmics: A high-throughput method for exploration of protein function in mammals. *Nat. Methods* **5**, 409–415
49. Brouhard, G. J., Stear, J. H., Noetzel, T. L., Al-Bassam, J., Kinoshita, K., Harrison, S. C., *et al.* (2008) XMAP215 is a processive microtubule polymerase. *Cell* **132**, 79–88
50. Renna, C., Rizzelli, F., Carminati, M., Gaddoni, C., Pirovano, L., Cecatiello, V., *et al.* (2020) Organizational principles of the NuMA-dynein interaction interface and implications for mitotic spindle functions. *Structure* **28**, 820–829.e6
51. Chinen, T., Yamamoto, S., Takeda, Y., Watanabe, K., Kuroki, K., Hashimoto, K., *et al.* (2020) NuMA assemblies organize microtubule asters to establish spindle bipolarity in acentrosomal human cells. *EMBO J.* **39**, e102378
52. Kapoor, T. M., Mayer, T. U., Coughlin, M. L., and Mitchison, T. J. (2000) Probing spindle assembly mechanisms with monastrol, a small molecule inhibitor of the mitotic kinesin, Eg5. *J. Cell Biol.* **150**, 975–988
53. Alessi, D., Macdougall, L. K., Sola, M. M., Ikebe, M., and Cohen, P. (1992) The control of protein phosphatase-1 by targetting subunits. *Eur. J. Biochem.* **210**, 1023–1035
54. Ramkumar, A., Jong, B. Y., and Ori-McKenney, K. M. (2018) ReMAPping the microtubule landscape: how phosphorylation dictates the activities of microtubule-associated proteins. *Developmental Dyn.* **247**, 138–155
55. Borman, M. A., Freed, T. A., Haystead, T. A. J., and MacDonald, J. A. (2009) The role of the calponin homology domain of smoothelin-like 1 (SMTNL1) in myosin phosphatase inhibition and smooth muscle contraction. *Mol. Cell Biochem* **327**, 93–100
56. Lontay, B., Bodoor, K., Weitzel, D. H., Loiselle, D., Fortner, C., Lengyel, S., *et al.* (2010) Smoothelin-like 1 protein regulates myosin phosphatase-targeting subunit 1 expression during sexual development and pregnancy. *J. Biol. Chem.* **285**, 29357–29366
57. Scotto-Lavino, E., Garcia-Diaz, M., Du, G., and Frohman, M. A. (2010) Basis for the isoform-specific interaction of myosin phosphatase subunits protein phosphatase 1c beta and myosin phosphatase targeting subunit 1. *J. Biol. Chem.* **285**, 6419–6424
58. Zhang, J.-P., Li, X.-L., Li, G.-H., Chen, W., Arakaki, C., Botimer, G. D., *et al.* (2017) Efficient precise knockin with a double cut HDR donor after CRISPR/Cas9-mediated double-stranded DNA cleavage. *Genome Biol.* **18**, 1–18
59. Kiyomitsu, T., and Boerner, S. (2021) The nuclear mitotic apparatus (NuMA) protein: a key player for nuclear formation, spindle assembly, and spindle positioning. *Front. Cell Developmental Biol.* **9**, 1–12
60. Lewis, C. W., and Chan, G. K. (2018) 18 - role of cytoplasmic dynein and dynactin in mitotic checkpoint silencing. In: King, S. M., ed. Dyneins: Structure, Biology and Disease, Second Edition, Academic Press, Massachusetts: 516–533
61. Liu, C., Shi, Y., Li, J., Liu, X., Xiahou, Z., Tan, Z., *et al.* (2020) O-GlcNAcylation of myosin phosphatase targeting subunit 1 (MYPT1) dictates timely disjunction of centrosomes. *J. Biol. Chem.* **295**, 7341–7349
62. Fourest-Lieuvin, A., Peris, L., Gache, V., Garcia-Saez, I., Juillan-Binard, C., Lantez, V., *et al.* (2006) Microtubule regulation in mitosis: tubulin

phosphorylation by the cyclin-dependent kinase Cdk1. *Mol. Biol. Cell* **17**, 1041–1050
63. Trinkle-Mulcahy, L., Sleeman, J. E., and Lamond, A. I. (2001) Dynamic targeting of protein phosphatase 1 within the nuclei of living mammalian cells. *J. Cell. Sci.* **114**(Pt 23), 4219–4228
64. Ferrar, T., Chamousset, D., De Wever, V., Nimick, M., Andersen, J., Trinkle-Mulcahy, L., *et al.* (2012) Taperin (c9orf75), a mutated gene in nonsyndromic deafness, encodes a vertebrate specific, nuclear localized protein phosphatase one alpha (PP1α) docking protein. *Biol. Open* **1**, 128–139
65. Trinkle-Mulcahy, L., Chusainow, J., Lam, Y. W., Swift, S., and Lamond, A. (2007) Visualization of intracellular PP1 targeting through transiently and stably expressed fluorescent protein fusions. *Methods Mol. Biol.* **365**, 133–154
66. Fox, A., Mehta, V., Boulon, S., and Trinkle-Mulcahy, L. (2015) Extracting, enriching, and identifying nuclear body sub-complexes using label-based quantitative mass spectrometry. *Methods Mol. Biol.* **1262**, 215–238
67. Cox, J., and Mann, M. (2008) MaxQuant enables high peptide identification rates, individualized p.p.b.-range mass accuracies and proteome-wide protein quantification. *Nat. Biotechnol.* **26**, 1367–1372
68. Prévost, M., Chamousset, D., Nasa, I., Freele, E., Morrice, N., Moorhead, G., *et al.* (2013) Quantitative fragmentome mapping reveals novel, domain-specific partners for the modular protein RepoMan (recruits PP1 onto mitotic chromatin at anaphase). *Mol. Cell Proteomics* **12**, 1468–1486
69. Olivier, N., Keller, D., Rajan, V. S., Gönczy, P., and Manley, S. (2013) Simple buffers for 3D STORM microscopy. *Biomed. Opt. Express* **4**(6), 885–899